FINAL REPORT

SEISMIC RISK ANALYSIS FOR GENERAL ELECTRIC PLUTONIUM FACILITY PLEASANTON, CALIFORNIA PART II

TERA CORPORATION

FINAL REPORT

SEISMIC RISK ANALYSIS FOR GENERAL ELECTRIC PLUTONIUM FACILITY PLEASANTON, CALIFORNIA PART II

Submitted to:

University of California
Lawrence Livermore Laboratory
P.O. Box 808
Livermore, California 94550

Attention: Mr. Don Bernreuter, L-90
Project Manager

June 27, 1980

TERA CORPORATION

2150 Shattuck Avenue
Berkeley, California 94704
415·845·5200

Berkeley, California
Dallas, Texas
Bethesda, Maryland
Washington, D.C.
New York, New York
Del Mar, California
Baton Rouge, Louisiana

TABLE OF CONTENTS

1.0 INTRODUCTION AND SUMMARY

This report is the second of a two part study addressing the seismic risk or hazard of the special nuclear materials (SNM) facility of the General Electric Vallecitos Nuclear Center at Pleasanton, California. The Part I companion to this report, dated July 31, 1978, presented the seismic hazard at the site that resulted from exposure to earthquakes on the Calaveras, Hayward, San Andreas and, additionally, from smaller unassociated earthquakes that could not be attributed to these specific faults. At the time the Part I study was initiated, it was believed that this formulation would account for all the significant earthquake loads that the site could experience. However, while this study was in progress, certain additional geologic information became available that could be interpreted in terms of the existence of a nearby fault. Although substantial geologic investigations were subsequently deployed, the existence of this postulated fault, called the Verona Fault, remained very controversial. The purpose of the Part II study was to assume the existence of such a capable fault and, under this assumption, to examine the loads that the fault could impose on the SNM facility.

Because of the proximity of the fault to the SNM facility, two types of loads are considered in this analysis. First, and compatible with the Part I report, we consider the vibratory loads that could be induced. The parameter used to characterize this load is the peak ground acceleration (PGA). In addition, we consider the possibility of earthquake rupture occurring directly under the facility by evaluating the possible rupture displacement load. For both types of loads, we approach the problem probabilistically so that our results will enable a designer or policymaker to set the design criteria consistent with levels accepted for other complex structures.

This report first reviews the geologic setting with a focus on specifying sufficient geologic parameters to characterize the postulated fault. The report next presents the methodology used to calculate the vibratory ground motion hazard. Because of the complexity of the fault geometry, a slightly different methodology is used here compared to the Part I report. This section ends with

the results of the calculation applied to the SNM facility. Finally, the report presents the methodology and results of the rupture hazard calculation.

It should be noted that although there are straightforward techniques available to combine the results in this study with those in the Part I report, such a combination is not recommended here. This is because the model for assessing the vibratory ground motion hazard in the Part I report included a background seismicity model that accounted for seismicity in the site vicinity. A simple combination of these results would, therefore, be conservative.

The results of our analyses are presented in Figures I-1 and I-2. These results indicate that a vibratory load of 30 percent g from the Verona Fault has a return period of 2,000 years, while a rupture displacement of one meter has a return period of 19,500 years. There are certain possible conservatisms contained in these results, presented in more detail in the text. Summarily, however, these include the following:

- The fault rupture model assumes that all ruptures occur on a single shear, and that Building 102 is located directly on top of that shear. There is, in fact, topographic evidence that the nearby H shears do not intersect the Building 102 foundation area, but instead pass to the south, thus further justifying the conservatism in assuming all future earthquake activity occurs directly under Building 102.

- Our analysis assumes that earthquakes of a given magnitude are uniformly distributed with depth over the fault plane. In fact, larger earthquakes are probably preferentially located deeper.

- The analysis uses a relation between magnitude and rupture displacement. The displacement values used in deriving this relation undoubtedly include some component of post-seismic slip that resulted from one or more creep events following the earthquakes. The desired, but unavailable data, is the coseismic slip.

- The seismotectonic data used as input to the hazard analyses are believed to be conservative; however there are insufficient data available to support better, mean-centered seismotectonic data.

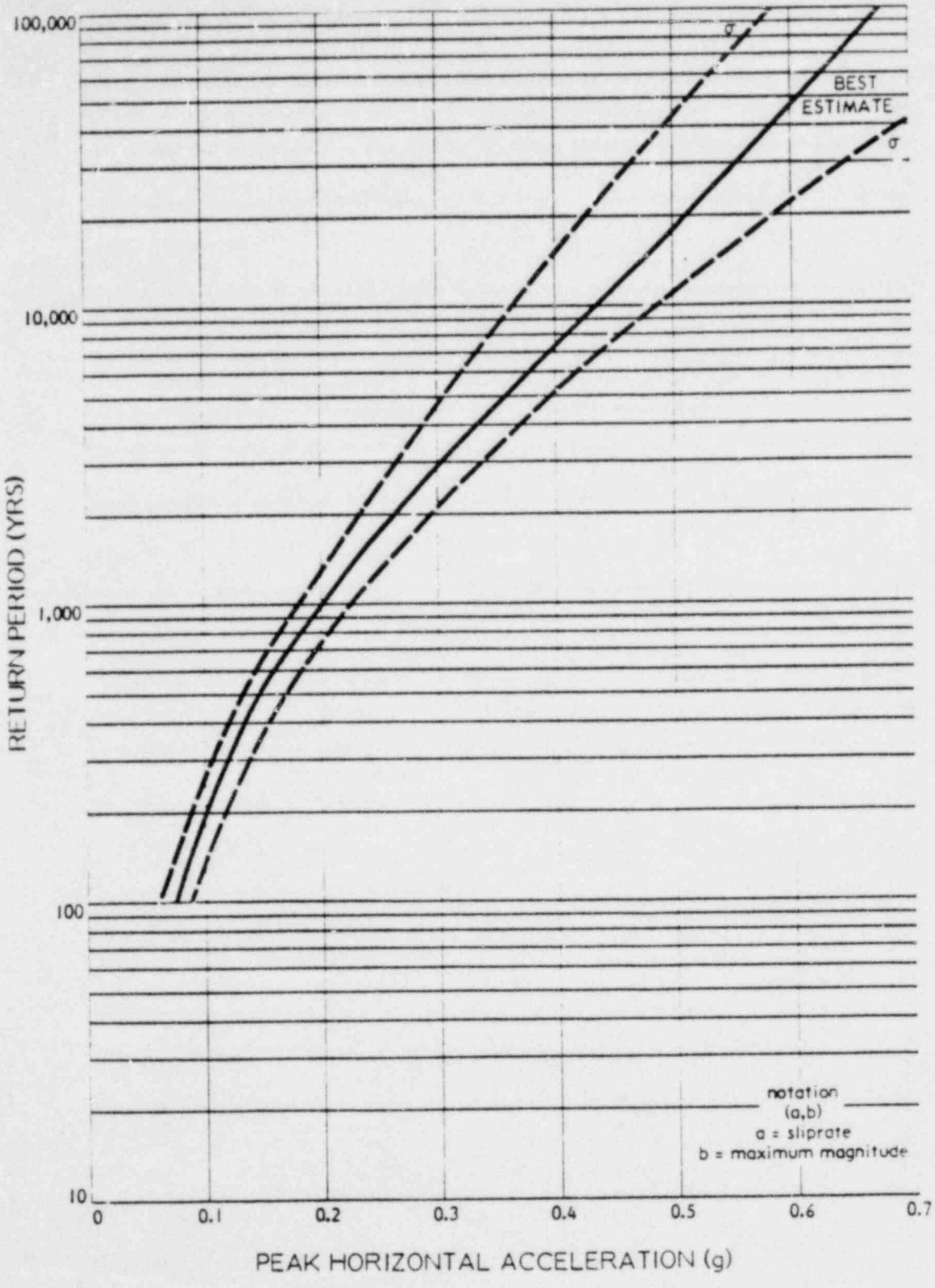

FIGURE 1-1

PEAK ACCELERATION V.S.
RETURN PERIOD FOR THE
SNM FACILITY

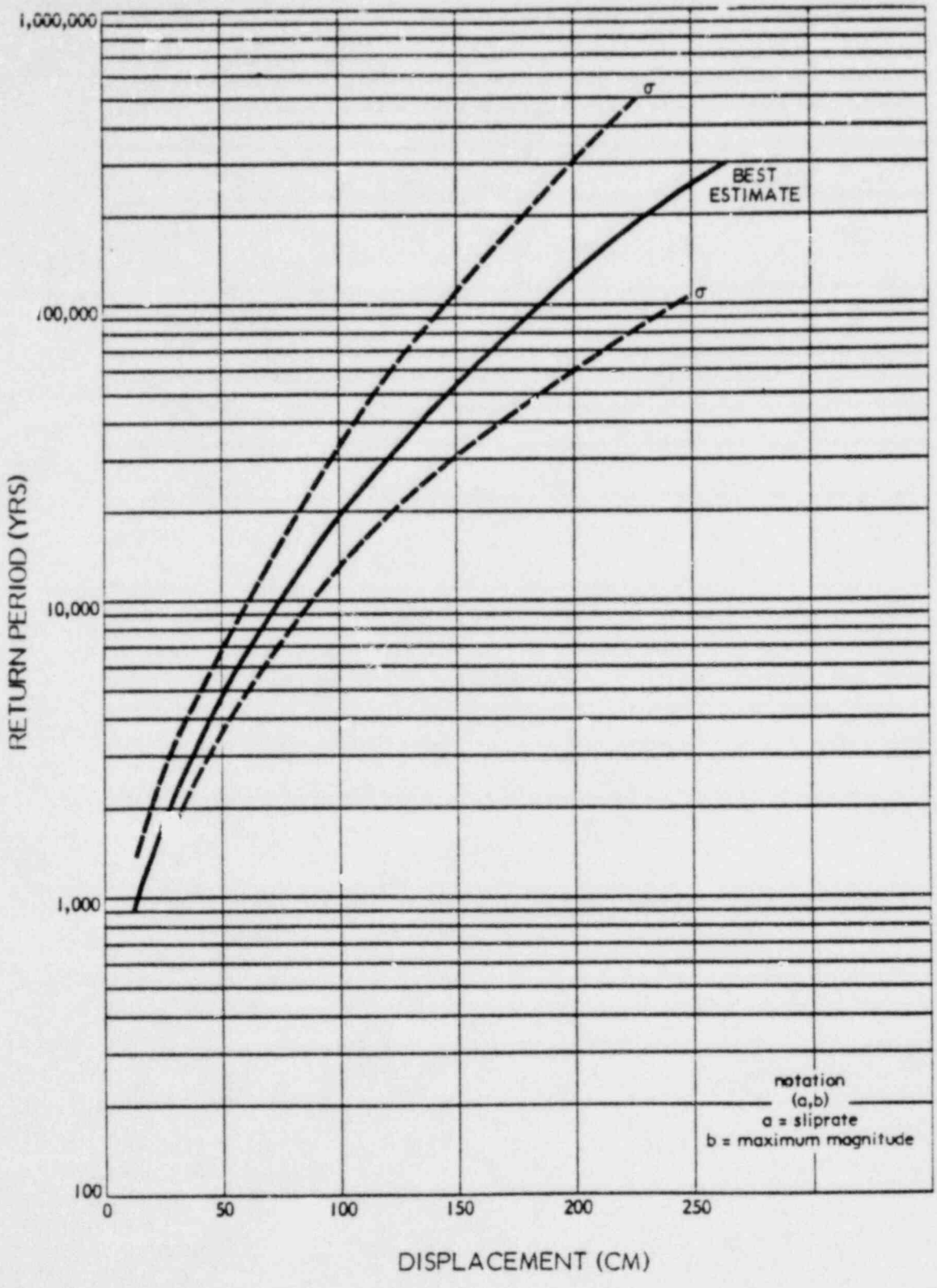

FIGURE 1-2

RUPTURE DISPLACEMENT V.S.
RETURN PERIOD FOR THE SNM FACILITY

On the other hand, we want to acknowledge certain weaknesses in this model as follows:

- No fault, particularly the Verona Fault, can be classed as uniquely thrust or otherwise. Because of this, we chose to include data from many types of earthquakes in our model building.

- Our earthquake occurrence model for the Verona Fault assumes that earthquakes of a given magnitude are equally likely over the fault's length. Although we consider this reasonable, it results in certain larger earthquakes rupturing beyond the "ends" of the fault. Other, more complex but no more reasonable, models could result in slightly greater predicted loads at the SNM facility.

- The model for earthquakes is based on a Poisson occurrence model which is time-independent. Although this is a conventional assumption, other models that include strain build-up and relaxation effects could possibly yield greater loads, depending on the time cycle.

- We have calculated the accelerations at Building 102 using an embedment model derived from actual acceleration data. A statistical analysis of this data, different from the one employed by us in this model, could yield different embedment models.

However, in our opinion, the uncertainty and conservatism in the seismotectonic input dominates any uncertainty associated with any of the above model inadequacies.

2.0 GEOLOGY AND SEISMOLOGY

2.1 REGIONAL GEOLOGY

Geological Setting

As shown in Figure 2-1, Vallecitos Valley lies between the Vallecitos Hills on the north and east and the Sunol Uplands to the south and west. This portion of the Central Coast Range of California is characterized by a relatively young stratigraphic sequence of sedimentary rocks and a complex tectonic framework. Bedrock, namely the Livermore formation that surrounds and underlies the valley, is of late Tertiary and Pleistocene age and has been folded and faulted between two major fault zones, the Calaveras and Greenville faults. These major faults are associated with the San Andreas system and constitute a portion of the boundary between the Pacific and North American Plates. Right lateral strike slip movement on the active Calaveras fault, located immediately west of the Vallecitos Valley, appears to have created northeast-southwest compressional forces resulting in the uplift of the highlands surrounding the valley.

Geomorphically, the valley and uplands are of low to moderate relief with landforms depicting youthful stages of development. The uplands form rounded smooth moderate slopes and V-shaped intervening drainages that are actively eroding headward and downward. Ancient and modern landsliding is common in many of the more precipitous slopes. The degradation of the uplands is forming small alluvial fans and colluvial deposits on the low relief valley floor. Predominantly southwest flowing drainages on the valley floor have incised the modern surface where modern soils are slowly being developed.

The study area lies within the Alameda Creek Watershed that lies above Sunol Dam. Streams in the Vallecitos Valley are intermittent and flow southwest into Arroyo de la Laguna. Several perennial springs are located on the major stream floors within the Vallecitos Hills. The groundwater table beneath the valley floor varies from an estimated 50 to 150 feet below the ground surface.

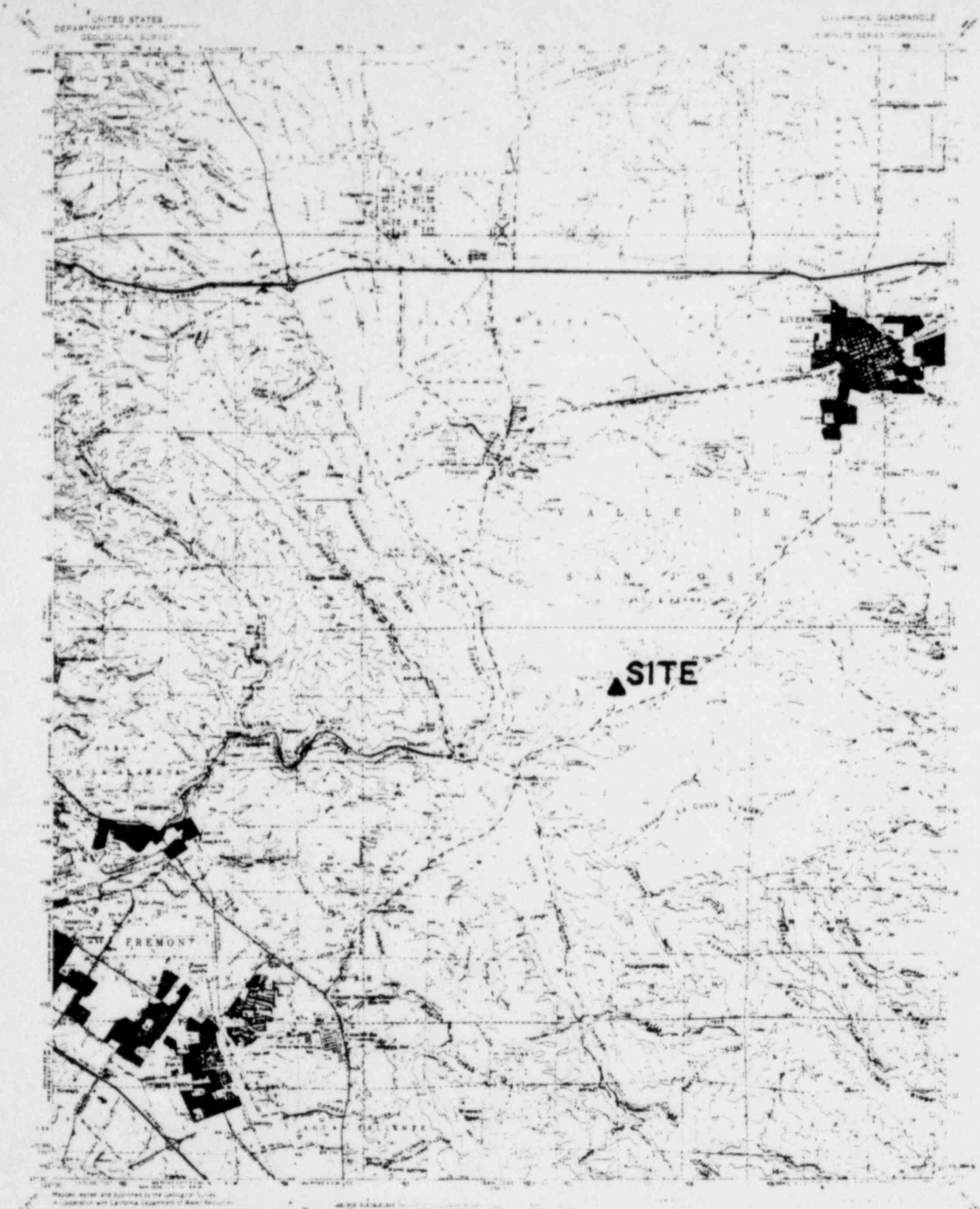

FIGURE 2-1

TOPOGRAPHY OF THE
SITE VICINITY

TERA CORPORATION

Bedrock

The Vallecitos Valley is essentially surrounded and underlain by interbedded gravel, sand, silt, and clay beds and lenses belonging to the Livermore formation. The older, middle and younger members range in age from an estimated 4.2 million to 1 million years. The formation may attain a thickness of 2,000 feet in the Vallecitos Valley and thickens eastward to as much as 8,000 feet near the center of the adjoining Livermore Valley to the east.

Upper Miocene age rocks and Cierbo and Briones sandstones of unknown thickness probably underlie the Livermore formations within the valley. In turn, the Miocene rocks are underlain by rocks of the Great Valley Sequence (Cretaceous) and/or Franciscan assemblage (Jurassic).

The floor of the Vallecitos Valley has a thin mantel of colluvial and paleosol deposits. Young fan deposits are built over older fans along the northeast side of the valley. Recent stream alluvium has accumulated in the larger drainages within the hills and on the valley floor. Slope wash and landslide debris cover most of the slope areas around the valley.

Structure

The regional tectonic fabric (Figure 2-2) is complex and generally consists of northwest-southeast trending folds and faults, inclusive of the Calaveras, Livermore and Greenville faults. Within the Vallecitos Valley is the northwest trending Verona Fault which displays reverse dip slip movement and dips to the northeast. The fault trace traverses along the southwest front of the Vallecitos Hills from Highway 84 northward to the town of Pleasanton, about five miles in lenght. Associated with the Verona Fault are at least two minor subparallel shears located in the valley southwest of the main trace. These two shears (known as B-2 and H) can be measured in hundreds of feet in length and also display predominately reverse dip slip movement. The main Verona Fault and the two subsidiary shears, B-2 and H, are believed to be part of the same fa. zone and are probably connected at depth.

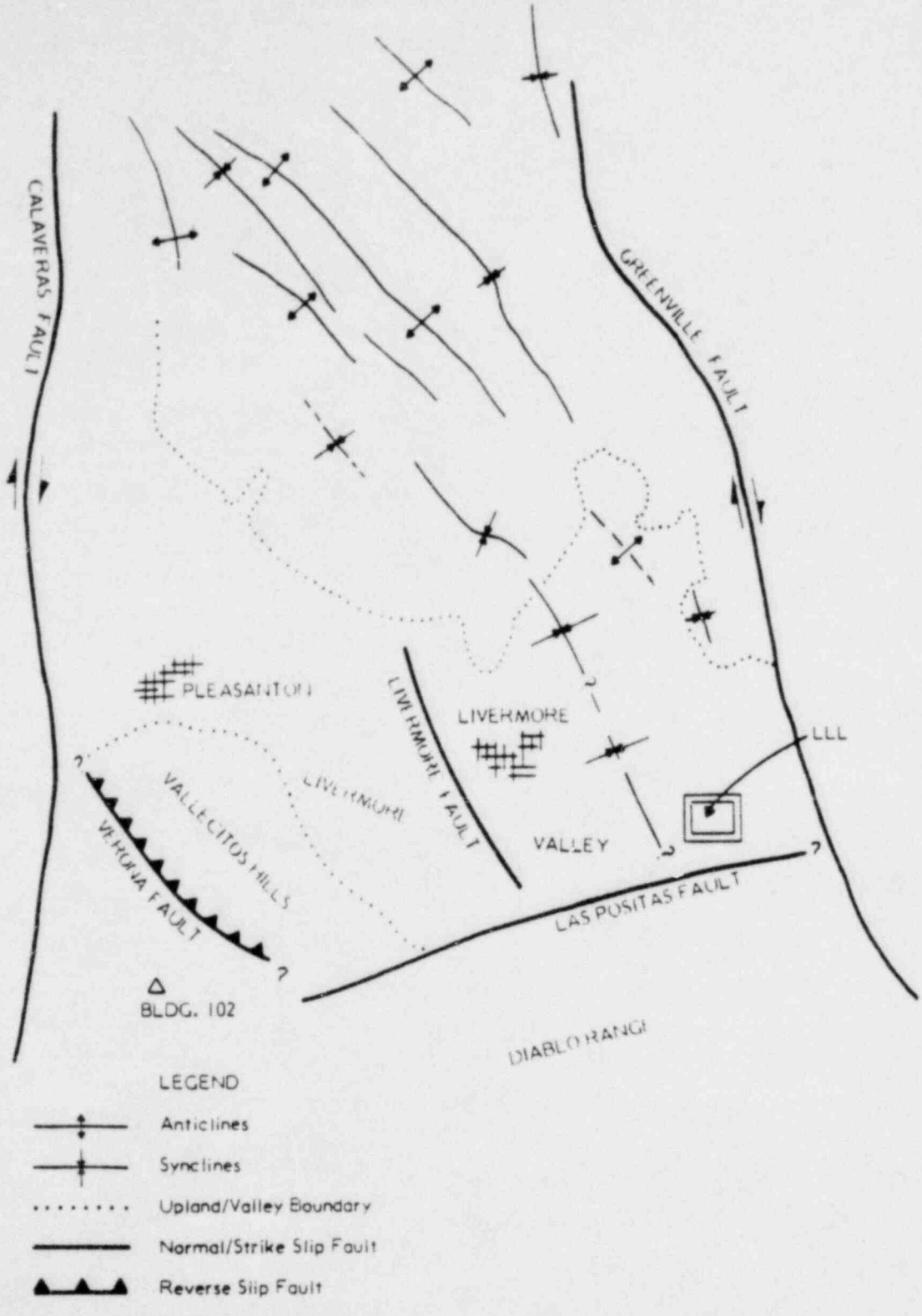

FIGURE 2-2

MAJOR TECTONIC FEATURES
LIVERMORE VALLEY REGION

There are conflicting concepts for the origin of the shears mapped within the Vallecitos Valley. The observed shears can be explained by both a landslide and a fault theory. The pros and cons for each have been addressed in detail through previous investigations (ESA, 1979). For this study the model for faulting was conservatively assumed.

Both the main trace of the Verona shears and the subsidiary shears (B-2 and H) have been well documented where observed by previous investigations (ESA, 1979). We feel that the trenching, boring and mapping of the shears have provided a reasonable characterization of the features in terms of the ages of last movement and the amounts of displacement.

Another major fault that was mapped by Herd (1977) trends into the southeastern portion of Vallecitos Valley. This fault is known as the Las Positas Fault and extends from the Greenville Fault, along the southern margin of the Livermore Valley across the Vallecitos Hills. At this time, field work including trenching and mapping is being conducted to help determine the fault's characteristics. It should be noted that during or after the Greenville Earthquake sequence of January 1980, ground cracking was observed at three locations south of the Lawrence Livermore Laboratory along the inferred trace of the fault. This most recent information suggests the Las Positas Fault might be capable of generating an earthquake and subsequent ground breakage.

2.2 SITE SPECIFIC-GEOLOGY BUILDING 102

Building 102 is situated near the center of the Vallecitos Valley, approximately 2,400 feet southwest of the base of the Vallecitos Hills and Verona Fault trace. A roughly eliptical shaped hill lies immediately east of the Building 102 complex. This hill is about 1,600 feet long (northwest-southeast trend), 1,200 feet wide and reaches an elevation of 583 feet, some 130 feet above the building complex.

Active erosion on the hill is minimal and only one major southwest flowing drainage has slowly disserted the central portion. In profile the hill is assymetrical with the southern flank slightly steeper than the northern flank.

Slopes range from 2:1 (horizontal to vertical) to 4:1 and are well rounded and smooth. The slopes are covered with low grass and appear to have been cultivated at one time or another. Terrain surrounding the hill is of low relief with a very shallow southwest sloping surface.

The southwest flank of the hill is roughly linear which could be structurally controlled by the aforementioned H-shear. Not shown on the more recent topographic maps is a small west trending spur ridge located at the extreme southwestern end of the existing hill. Air photos dated 1957 clearly show a small elongated ridge about 20 feet high extending about 400 feet to the west of the hill. This small ridge has since been removed by grading. The topographic high appears to be a continuation of the hill front that presumable was the previous location or extension of the H-shear. The distal edge of the spur prior to grading was about 280 feet south of the south edge of Building 102.

A shallow mantel of modern soil and slope-wash covers most of the slopes except for several small exposures of Livermore gravel observed along the western margin of the hill. The hill has been mapped (ESA, 1979) as Younger Livermore Gravels consisting of alternating and merging of gravel, sand, silt and clay beds and/or a combination of these materials.

Structurally, the bedrock is believed to dip southward at about 30 degrees and generally strikes northwest, at least along the southwest portion of the hills. Examination of 1957 air photos shows what are believed to be bedding features and suggests that beds dip north near the central portion of the hill. It is possible the hill could represent a small fold, suggesting that the uplift of the hill would not be entirely due to faulting.

Shear H was well documented in Trench H (210 feet long) and its two-side trenches (H-1 and H-2) by ESA (1979). The trench was located about 400 feet southeast of Building 102 and trended in a north-south direction normal to the shear. The trench was excavated to a depth of about 15 feet with a 30-foot width.

Basically, as observed in Trench H, Younger Livermore Gravels had been thrust over at least four buried paleosol horizons along a 5 to 10 foot wide zone consisting of one main and several small shears. The shears displayed slickensides that indicate mostly dip slip movement and minor left lateral oblique displacement. The stirke of the shear zone was about normal to the trend of the trench (N85°W) and dipped northward at 20 to 30 degrees. Similar displaced materials on either side of the shears wre not found. Based on the geometry of the shear a total of 30 feet of throw was evident when measured in the trench.

The four buried paleosols observed in the trench were estimated to have been formed during oxygen isotope stages 5, 7, 9 and 11 which date from 70,000 to 450,000 years before present (ESA 1979). The Younger Livermore Gravels are believed to be at least 1,000,000 and probably more like 2,000,000 years old. No data were found in any of the three trenches, from which to obtain minimum ages of last movement on the shears. Unfortunately, the modern surface soils at the bedrock surface had previously been distrubed by tilling.

For this study, and from the data available, the shear observed in Trench H is continuous along the southern front of the hill for about 2,400 feet. There is no mapped geologic or geomorphic evidence to suggest that Shear H is continuous in either direction of the hill or merges with other surface structures such as Shear B-2 or the Verona Fault. At the surface, Shear H is considered to be a separate entity; however, we feel that the H, B-2 and Verona most likely merge into one feature at depth.

There is the possibility that Shear B-2 could continue southeastward from its last known location (Trench B-2-2) and extend along the northeast side of the hill; however, this is difficult to explain based on the known direction of movement along Shear B-2.

2.3 FAULT PARAMETERS

To determine the fault parameters of the Verona fault system, the geologic history during the Late Quaternary of the region had to be simplified. Several

points are summarized below that help establish minimum and maximum ages during which it is estimated that faulting commenced in the Vallecitos Valley.

1. There is general agreement that the Livermore gravels (youngest to oldest members) were deposited 4.2 to 1.0 million years before present (B.P.). It is further assumed that the Livermore gravels were deposited in a continental alluvial outwash environment and beds were deposited at low bedding dip angles (e.g., < 5 degrees). During filling of the central Livermore basin area, subsidence was initiated and continued as deposition progressed. As much as 8,000 feet of valley fill now exists in the central portion of Livermore Valley.

2. Regional geologic mapping of the site area indicates that all members of the Livermore gravels are tilted toward the northeast and apparently even the youngest gravels are deformed as much as the older members. This suggests that structural folding commenced after deposition of the gravels was complete, about 1.0 million years before present. Some of the eastward tilting can be attributed to depositional subsidence; however, anticlines and synclines within the youngest gravels suggest that compressive forces have been active in the last 1.0 million years B.P.

3. Structural folding continued up to the time of the development of the paleosols in the Vallecitos Valley because the paleosols do not appear to be deformed by folding. The oldest paleosol in the Vallecitos Valley is believed to be about 400,000 to 500,000 years old.

4. The faulting process could have commenced at the time compressional folding started since both types of deformation are compatible and were produced by northeast-southwest compressional forces. If this is the case, then a maximum conservative limit for the start of faulting is about 1.0 million years B.P.

5. A minimum limit as to when faulting started can be established if we assume that faulting commenced after the folding process stopped (e.g.,

400,000 to 500,000 years B.P.). The compressional forces in the area causing folding were transformed into a faulting mode that subsequently resulted in at least partial uplift of the Vallecitos hills.

6. It is possible that faulting could have started even later than the period of paleosol development, however, the slip rates for the Verona fault become excessive based on the assumed amount of displacement.

The minimum and maximum dates for when faulting started (500,000 and 1,000,000 years B.P.) are considered realistic, although conservative. The reason they are considered conservative is because additional geologic processes had to have taken place within the same time frame. A period of extensive erosion and perhaps mass wasting was necessary to account for the stratigraphic section (Livermore gravels) that is now missing west of the Verona Fault. The stratigraphic section through the Valecitos Hills is at least 5,000 feet thick. The section west of the Verona Fault is estimated to be 2000+ feet thick, leaving about 3000 feet of gravel to be removed. This projected section represents several cubic miles of gravels that were eroded and removed entirely from the Vallecitos Valley area. The erosion process had to have occurred in the last 1.0 million years since the last gravels were deposited.

With this in mind it is hard to believe that the paleosols could have survived this vast erosion process on the Vallecitos Valley floor. It is difficult to believe that the paleosols are representative of the stable landscape periods between great periods of erosion and removal. Since the paleosols are well preserved and thinly stacked one upon the other the unstable periods of erosion between their development must have been minor. If this is correct then the great erosion period had to have occurred sometime between 1.0 million years B.P. and the development of the paleosols (400,000 to 500,000 years B.P.).

The apparent discrepancy for the occurrence of the above stated processes is best explained by an incorrect assumed age of the youngest Livermore Gravels (e.g., one million years). Two million years is a more reasonable period for the occurrence of the faulting, folding and erosion.

In summary, vast erosion along with the folding and faulting, portions of which may have occurred simultaneously, occurred in the last 1.0 million years and more realistically in the last two million years. It is our opinion that the slip rates described below are conservative because it is very difficult to conceive that all of these processes took place in such a short (geologically) time span. It should be noted, however, that there is insufficient data available to enable us to remove the conservatism in slip rates.

Slip Rates Verona Fault System

As presented in Figure 2-3, the slip rate for the Verona Fault was established using a model based on the estimated amount of throw along the fault. A throw of 900 feet was calculated utilizing the elevation difference between the top of the Vallecitos Hills (≈1300 feet) and the toe of the Hill (≈600 feet). A near surface fault dip angle of 26 degrees (bedding plane fault) that steepens to 60 degrees at depth was considered. The preceding section discussed ages of when faulting commenced on the Verona Fault. It is our best, although conservative, estimate that faulting started about 1.0 million years B.P. and has continued up to at least the Middle Holocene period.

There is a realistic probability that a portion of the Vallecitos Hills uplift was a result of not only faulting, but folding and erosion (downcutting) of the valley floor. The following conservative slip rate is realized not considering that other processes contributed to the uplift of the Vallecitos Hills:

- 900 feet of throw
  have occurred in 1.0 million years = 0.03 cm/yr

Assuming a reasonable 80 percent of uplift was due to faulting and 20 percent was due to other processes, the following more reasonable slip rate is established:

- 650 feet of throw
  have occurred in 1.0 million years = 0.02 cm/yr

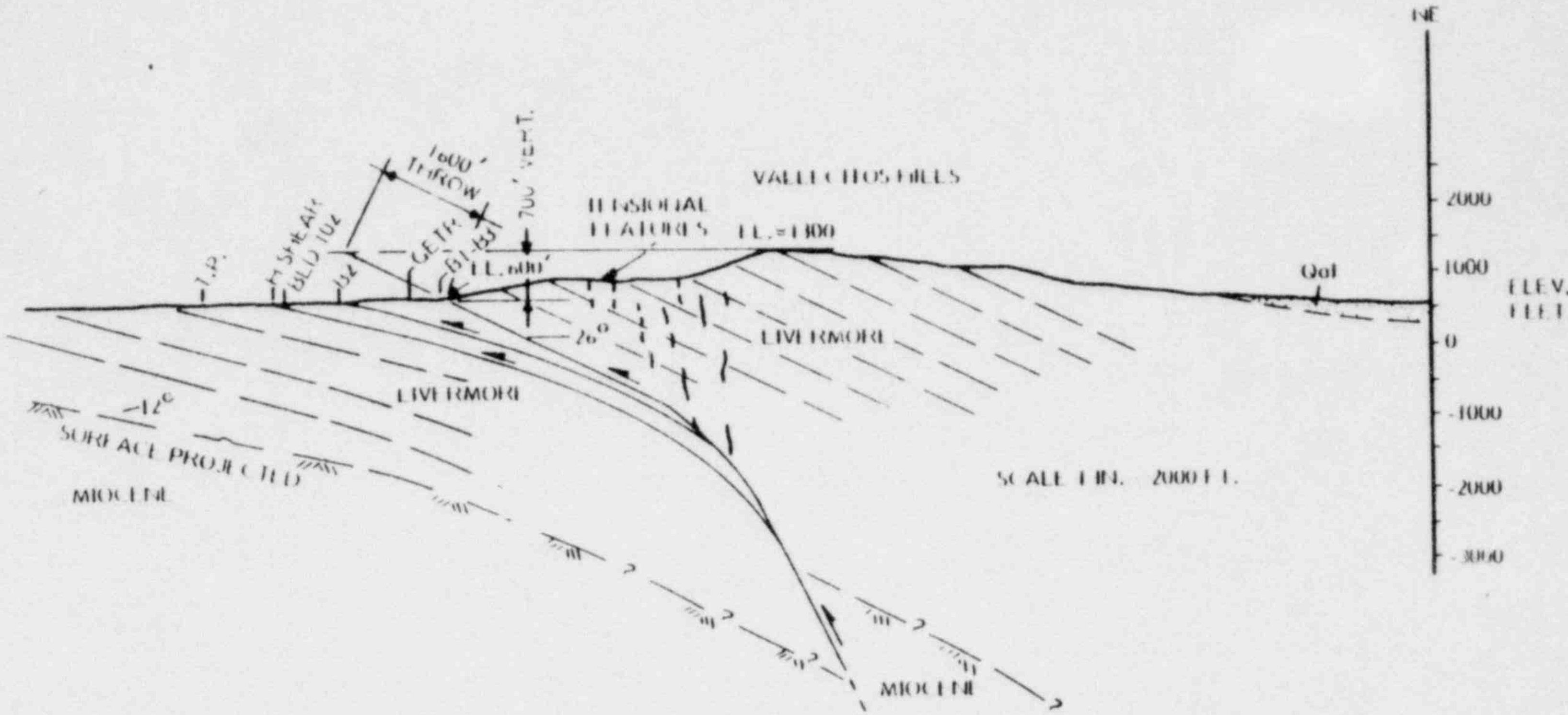

FIGURE 2-3

MODEL FOR BEDDING PLANE FAULT
SECTION DRAWN THROUGH GETR BEARING N40°E

For this analysis, it is our opinion that the .02 cm/yr slip rate is reasonable. An alternative slip rate model could be developed assuming that faulting commenced two million years ago. This results in one-half of the above slip rates.

The slip rate for Shear H near Building 102 was determined in a similar manner using maximum relief of the hill north of the shear. A maximum estimate of 100 feet of uplift has occurred resulting in 320 feet of throw on a 25 degree north dipping fault plane. Assuming the hill was uplifted entirely by faulting, and movement commenced 1.0 million years ago, a slip rate of 0.01 cm/year is calculated. Assuming 80 percent of uplift was due to faulting, and 20 percent to other processes, a throw of 195 feet is realized that would result in a slip rate of 0.006 cm/yr. This establishes the potential conservatism in using 0.02 cm/yr in the rupture hazard analysis for Building 102.

Recurrence Intervals

The same topographic model used to determine slip rates was employed to calculate recurrence intervals on the Verona fault. The following relationships were used:

$$\frac{\text{maximum amount of displacement (throw)}}{\text{single event displacement}} = \text{Number of events}$$

and

$$\frac{\text{total time period of faulting}}{\text{number of events}} = \text{Recurrence Interval (in years)}$$

The results of the trenching operation indicate that one to two and one-half meters of displacement have occurred on the shears of the Verona fault system during any one event. The following recurrence intervals are calculated:

With 1 meter displacement per event

$$\frac{1{,}600 \text{ feet throw}}{3 \text{ feet disp.}} \approx 500 \text{ events}$$

and

$$\frac{1{,}000{,}000 \text{ years}}{533 \text{ events}} \approx 1{,}900 \text{ years}$$

With 2 1/2 meters of displacement

$$\frac{1{,}600 \text{ feet throw}}{9 \text{ feet disp.}} \approx 200 \text{ events}$$

and $$\frac{1{,}000{,}000 \text{ years}}{178} \approx 5{,}600 \text{ years}$$

The intervals calculated above assume that uplift was entirely due to faulting. If 80 percent of uplift is assumed due to faulting and 20 percent due to other processes, the following recurrence intervals are realized:

With one meter displacement per event and 1,200 feet of throw:

$$\frac{1{,}200 \text{ feet throw}}{3 \text{ feet disp.}} = 400 \text{ events}$$

and $$\frac{1{,}000{,}000 \text{ years}}{400 \text{ events}} = 2{,}500 \text{ years}$$

With 2 1/2 meters displacement per event and 650 feet of throw:

$$\frac{650 \text{ feet throw}}{9 \text{ feet disp.}} = 72 \text{ events}$$

and $$\frac{1{,}000{,}000 \text{ years}}{72} = 13{,}889 \text{ years}$$

Fault Length

The lengths of the Verona and Las Positas faults have been in question. Actual fault lengths or whether the faults merge or terminate short of each other cannot be determined from the geologic data provided by ESA (1979) and Herd (1977).

In referring to Figure 2-4, a feature that could be interpreted as the Verona Fault can be well documented from field and air photo evidence, extending from locations B-C (2.4 km). On the basis of geomorphic and subsurface evidence, this represents the actual known total length of the postulated Verona fault. Northwesterly from B toward Pleasanton, it is hypothetical that the fault is

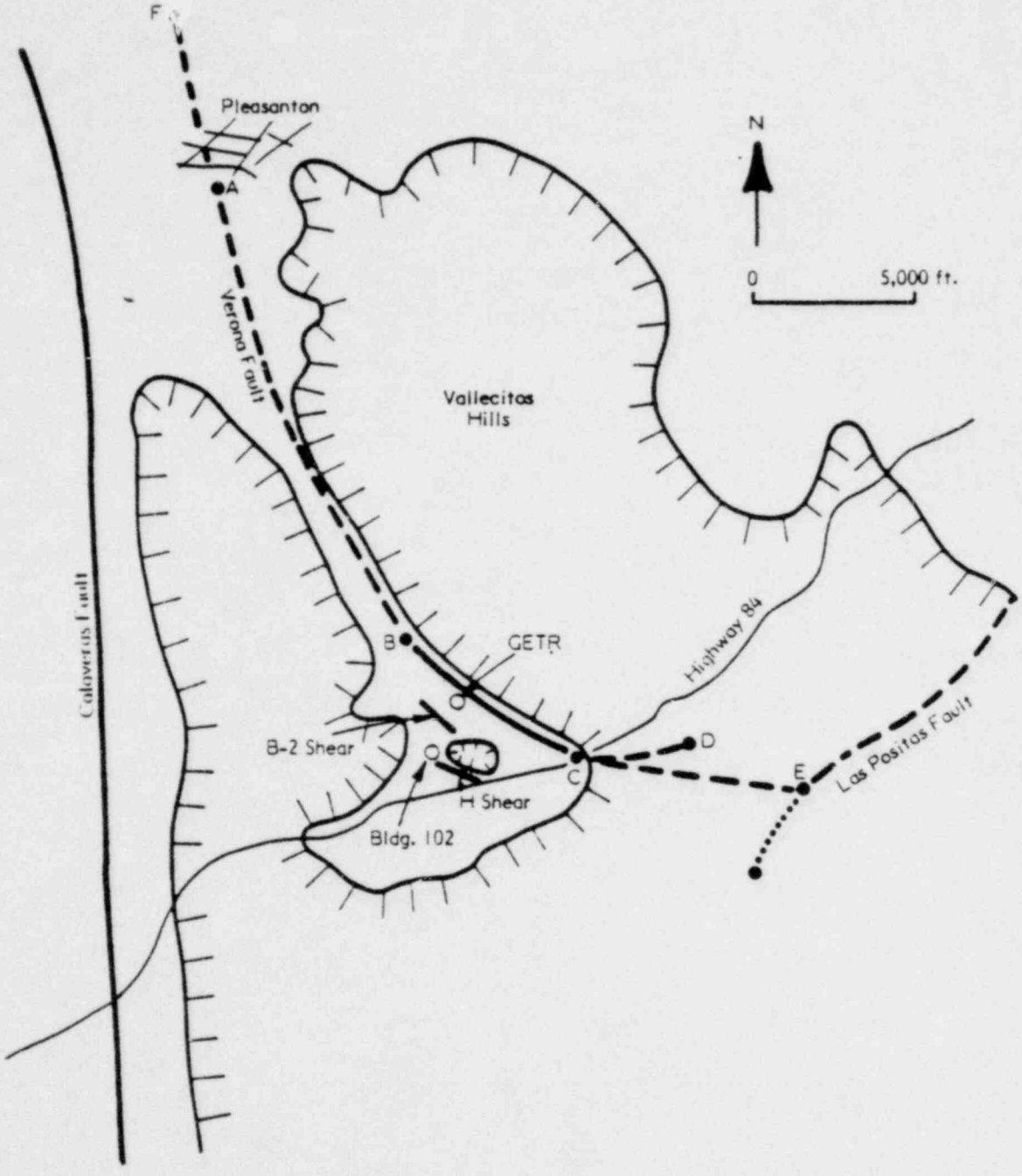

FIGURE 2-4

FAULT LENGTH

continuous. However, assuming the Vallecitos Hills were uplifted along the Verona Fault by compressional forces, the fault could continue to Location A. Position A is about the northern limit of the hills. Geologic data do not favor the Verona Fault continuing southeasterly past Highway 84 toward the Las Positas Fault. It is our opinion that the Verona Fault terminates near Highway 84. The fault length from A to C is about 7.2 km. There is a remote possibility the fault could continue northwesterly from Point A to Point F for an assumed distance of 1.5 km beneath the alluvium. Subtle geomorphic data suggest to us that the Verona Fault might terminate near Point D. A total Verona Fault length (F to D) of approximately 11.0 km is obtained as the reasonable upper limit to the fault length.

Evidence to merge the Verona Fault with the postulated Pleasanton Fault or the Calaveras Fault is lacking. It is our opinion that the Verona Fault is a separate feature and is responsible, in part, for the uplift of the Vallecitos Hills along their southwestern front. We further believe that much of the uplift of the hills from about points B to A is a result of folding.

The Las Positas fault as mapped by Herd (1977) is about 13 km long. There is fair to excellent evidence to suggest the fault trends from the eastern side of the Livermore Valley southwestward to about Arroyo Valle. From here the continuation of the fault toward the west is based on conjecture. For this study the approach is to use the fault length as mapped by Herd (1977).

As mentioned above it is our opinion the Verona Fault terminates at its southeastern end. No geologic evidence to date has been presented to suggest that the Verona and Las Positas faults merge into one through-going feature, although it cannot be ruled out. For the benefit of this study, if the two faults merge they most likely merge near Point E. The combined length of the two faults would be about 23 km.

In summary, the range of fault lengths considered appropriate for the Verona Fault are as follows:

Verona Fault (adequate field evidence)	2.6 km
Verona Fault (projected trace)	10.4 km
Las Positas Fault	13.0 km
Combined Verona and Las Positas faults	23.4 km

Fault Dip Angle

It has been suggested that the Verona Fault is a bedding plane fault. This has not been confirmed; however, a model for bedding plane faulting fits the field evidence as well as a steeper dipping fault plane model. A bedding plane fault can be a result of folding and not deep-seated crustal instability. For example, during the compressional folding of a syncline, the younger overlying beds tend to slip past one another in an apparent lengthening or thrusting action. This is considered structural deformation by faulting, but the faults move in response, perhaps slowly and periodically, to a slow folding action or creep. It is doubtful that this type of faulting is capable of producing an earthquake. Since this cannot be easily confirmed, a steeper dipping fault plane model was conservatively assumed.

As shown in Figure 2-5 the dip angle of the Verona Fault plane was estimated by using the location of known epicenters east of the fault trace and estimated depths. The Livermore Fault was considered a limiting factor in that the Verona Fault probably does not penetrate the near vertical Livermore fault plane.

One roughly linear epicentral trend lies about 3.2 km east of the Verona Fault and another 9 km to the east essentially located over the trend of the Livermore Fault. It is slightly possible that either of the linear epicentral trends represent earthquakes on the Verona Fault; therefore, we use these data in developing a fault dip model. Depths of 8 km for shallow earthquake and 15 km for deep earthquakes were assumed in determining the dip angle of the Verona fault plane.

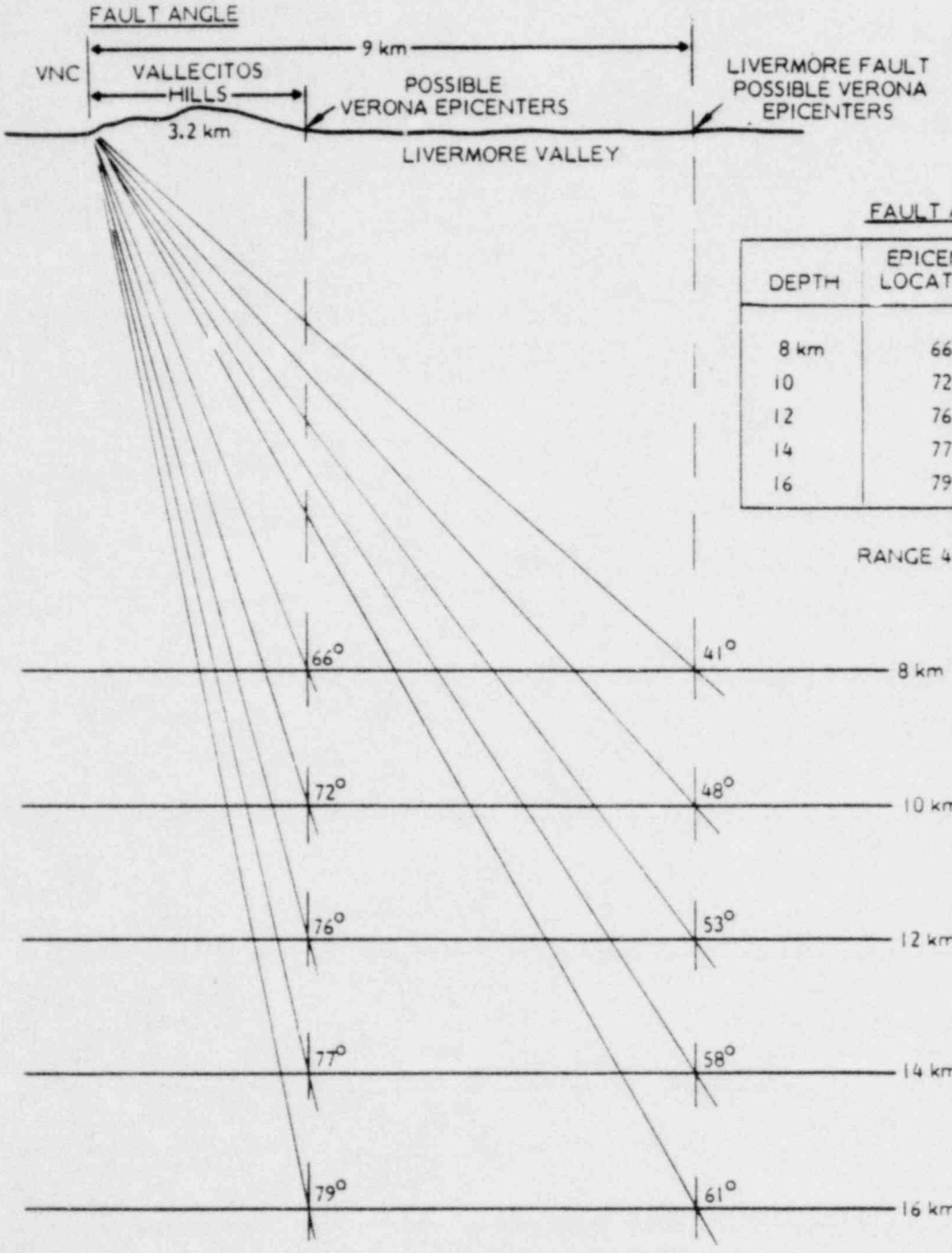

FAULT ANGLE

DEPTH	EPICENTER LOCATION A	EPICENTER LOCATION B
8 km	66°	41°
10	72	48
12	76	53
14	77	58
16	79	61

RANGE 41° to 79°

FIGURE 2-5

FAULT ANGLES (DEPTHS) ESTIMATED USING EPICENTER LOCATIONS
(FIG 3 HERD 1942-1968 1.5 M+)

Considering the above numbers, fault dip angles vary from 41 to 79 degrees. The geometry of the inferred fault planes is shown on Figure 2-5.

Using a dip angle of 26 degrees for the Verona Fault, as suggested in the slip rate calculations, would place the epicenter locations on the Verona Fault approximately 18 km to the east of VNC for shallow (eg. 8 km) earthquakes. This is not considered valid or realistic. In the case of the Verona, B-2 and H shears, the fault planes are shallow, near the surface and increase in dip angle with depth. A 60 degree dip angle is considered reasonable for this study. This would place shallow earthquake (8 km) epicenters about 4 km east of VNC and deep earthquakes (15 km) about 9 miles to the east.

2.4 MAXIMUM MAGNITUDES - VERONA FAULT

In this study, consideration was given to the length of the Verona Fault, amount of apparent single event displacements, the type of fault movement and the seismic history of the fault. These data are needed to help determine a maximum magnitude. Since there is a lack of a historic seismic history along the Verona Fault, geologic and empirical data were used to establish limits. A hypothetical fault length was suggested earlier of about 11 km using a conservative overrun at both ends of the fault. A more realistic fault length of 7.5 km is equal to about the length of the Vallecitos hills from Pleasanton to Highway 84. This is the segment considered most likely to break since it corresponds to the topographic expression of the scarp and/or distal edge of the fault. At least one meter of displacement was recorded in trenches near the General Electric Test Reactor (GETR) which is located below the highest hill top in the Vallecitos Hills (e.g., 1,285 feet). The north end of the hills attains a maximum elevation of 800 feet or about 400 feet above the valley floor. There is appreciably less apparent maximum uplift than at the southeast end near GETR. From this we rationalize that displacement may vary by 50 percent along the fault trace (e.g., 0.5 to 1.0 meters). This might further be explained by assuming that only portions of the fault move during a single event. The following data summarize the various magnitudes, based on empirical relationships from fault lengths and amount of displacement on the Verona fault.

Fault Length	11 km	7.5 km
Slemmons (1977)	7.0 M	6.8 M
Greensfelder (1972)	6.3 M	5.9 M
Bonilla and Buchannon (1970)	5.8 M	5.4 M

Displacement	1 meter	0.5 meter
Slemmons (1977)	7.0 M	6.8 M
Bonilla and Buchannon (1970)	6.9 M	6.1 M

Assuming that only one-half (normal practice) of the fault length was to rupture during a single event, we determined the following magnitudes:

Fault Length	0.5 x 11 km = 5.5 km
Slemmons (1977)	6.75 M
Bonilla and Buchannan (1970)	5.0 M
Greensfelder (1972)	6.1 M

It is difficult to assign a single maximum magnitude to the Verona fault. It is our opinion that only a portion of the fault will rupture the ground surface during an earthquake equal to about one-half the total length of the fault. Our best estimate for an earthquake magnitude on the Verona Fault is therefore 6.0.

It is also our opinion that the B-2 and H shears are not capable of producing an earthquake independently. It is reasonable to assume that the two shears move sympathically when the Verona fault moves.

2.. SUMMARY - FAULT PARAMETERS

In summary, based upon the data and the analysis presented above, we judge that the following data represent either reasonable or perhaps conservative best estimates and ranges of important input parameters to the calculations described in the remainder of this report.

Parameter	Best Estimate	Range	Units
Slip Rate	.02	.01 - .03	cm/yr
Fault Length	11.0	2.4 - 11	km
Dip Angle	60	41 - 79	degrees
Maximum Magnitude	6.0	5.5 - 6.5	M_L

2.4 SEISMICITY MODEL

This section presents the development of a seismicity model for the Verona fault that will be used in the fault hazard assessment. Conventional and desirable practice is to base seismicity models on the historical seismic record, although such as approach applied to the Verona Fault would be subject to unacceptable uncertainty due to the sparce seismic records. An alternative approach has been developed within the last several years that somewhat avoids this problem by relating certain geologic data to the earthquake process. The starting point, as outlined in Campbell (1977), is to relate the geologic slip rate on a fault with the occurrence of earthquakes. This model is developed below.

Brune (1968) has proposed an expression that can be used to estimate the total average slip $\langle u \rangle$ on a fault from the sum of seismic moments of earthquakes on the fault. This expression is given by:

$$\langle u \rangle = \frac{1}{\mu A_o} \sum M_o \qquad (2\text{-}1)$$

where μ is the shear rigidity of the medium, A_o is the total area of the fault zone given by its length L_o times its width W_o, and M_o is seismic moment defined as $\mu A \bar{D}$, (where A is the area of fault rupture for the event and $\bar{D}$ is the mean displacement).

Equation 2-1 can be generalized to establish a relationship between number of events having magnitudes m and greater, N(m), and the slip rate S_R. The total slip per year that can be expected to result from the occurrence of earthquakes on the fault can be given by:

$$S_R = \frac{1}{\mu A_o} \int_{-\infty}^{M_u} M_o(m) \quad |dN(m)| \tag{2-2}$$

where M_u is the upperbound magnitude on the fault, and $dN(m)$ is the number of events per year having magnitudes equal to m. The absolute value is required because the number of events decrease with increasing m, giving a negative slope for the N(m) versus m relation. In Equation 2-2 only the absolute number of events is required.

In order to analyze Equation 2-2, relationships among $M_o(m)$, $dN(m)$ and m are required. Let it be assumed that, for the fault, the number of earthquake occurrences per year of a given magnitude or greater can be given by the magnitude-frequency law,

$$N(m) = 10^{a-bm}; \quad m \leq M_u \tag{2-3}$$

Taking the derivative of this expression gives,

$$|dN(m)| = b \, \text{Log}_e 10 \; 10^{a-bm} dm \tag{2-4}$$

Let it also be assumed that the seismic moment of an event can be related to its magnitude by a relationship of the form,

$$M_o(m) = 10^{C_1+C_2 m} \tag{2-5}$$

which has been suggested from both empirical and theoretical considerations.

An expression for slip rate is obtained by substituting Equations 2-4 and 2-5 into Equation 2-2 and integrating, thus obtaining,

$$S_R = \frac{b}{(C_2-b)\,\mu A_o}\ 10^a\ \left[M_o(M_u)\ 10^{-bM_u}\right] \qquad (2\text{-}6)$$

An expression for the number of events per year of magnitude greater than or equal to m may be obtained by solving this equation for 10^a and multiplying each side by 10^{-bm},

$$N(m) = \frac{S_r\,\mu A_o(C_2-b)}{M_o(M_u)b}\qquad 10^{b(M_u-m)} \qquad (2\text{-}7)$$

Similar models have been recently proposed and applied by Anderson (1979) and Molnar (1979).

In terms of an application of this model, the data required to estimate the seismicity of the Verona Fault are listed in Table 2-1. The values for slip-rate, upper bound magnitude, and fault length were taken as the best estimate of these parameters as discussed above. A lower band magnitude of 3.5 was selected to represent a threshold below which earthquake occurrences would have a negligible effect on the hazard results.

A relationship between seismic moment and magnitude was developed from 167 recorded seismograms from earthquakes of $2.0 < M_L < 6.8$ occurring in Southern California. Seismic moments were estimated by several investigators (see Campbell, 1977) who matched observed source displacement spectra with spectra determined from dislocation theory. A least-squares analysis of these data resulted in the following log-linear relationship:

$$\text{Log}_{10}\, M_o(m) = 16.3 + 1.41\ m \qquad (2\text{-}8)$$

where $M_o(m)$ is seismic moment in dyne-cm. The fit resulted in a standard error of 0.42 and a correlation coefficient of 0.95. Based on this equation, the seismic moment of the M_L 6.0 upper band earthquake is estimated to be 5.8×10^{24} dyne-cm.

TABLE 2-1

SUMMARY OF SEISMOTECTONIC DATA USED IN THE ESTIMATE OF SEISMICITY

Parameter	Symbol	Estimates
Slip-Rate (cm/yr)	S_R	0.02
Upper Bound Magnitude	M_U	6.0
Seismic Moment of M_U (dyne-cm)	$M_o(M_U)$	5.8×10^{24}
Lower Bound Magnitude	M	3.5
Fault Length (km)	L_o	7
Fault Width (km)	W_o	18
Fault Area (km^2)	A_o	193
Shear Rigidity ($dyne/cm^2$)		3×10^{11}
Seismic Moment Coefficient	C_2	1.41
Richter b-value	b	0.87
Seismicity (events/yr $\geq M_\ell$)	$N(M_\ell)$	0.185

The fault width (W_o) is the distance from the surface to the maximum depth of faulting as measured along the dip of the fault plane. The maximum depth of faulting for the Livermore area is probably less than or equal to about 15 km, based on the maximum depth at which earthquakes are found to occur (Bolt and Miller, 1975). From this and the three-dimensional geometry of the Verona Fault, the fault width was estimated to be 18 km and the area of the fault plane to be 193 km^2.

A b-value of 0.87 was adopted from Campbell (1977) to be consistent with the seismicity of active regions within the western United States.

The remaining seismotectonic data used in the estimate of seismicity are presented in Table 2-1. Based on equation 2-8, the recurrence curve for the Verona Fault was determined as follows:

$$\text{Log}_{10} N(m) = 2.312 - 0.87\, m \qquad (2\text{-}9)$$

This corresponds to 0.185 events per year of magnitude greater than or equal to 3.5, or roughly one event every five and one-half years.

3.0 VIBRATORY GROUND MOTION HAZARD

The probability that the peak acceleration (A) is greater than some specified value (a) can be fundamentally represented by the total probability theorem

$$P\left[A > a\right] = \iint P\left[A \quad a/m \text{ and } r\right] f_M(m) f_R(r)\, dm dr$$

where P indicates probability, A a is the event whose probability is sought, and M and R are the continuous, independent random variables of magnitude and distance which influence A. The probability that A a will occur can be calculated by multiplying the conditional probability of A a (given m and r) times the probabilities of m and r, and integrating over all the possible values of m and r.

In describing the seismicity of the sources, we are hindered by incomplete and inaccurate historical data that are limited to a short time span. Reliance on frequency data alone can result in erroneous conclusions. For this reason, we base our analysis on geological and seismological data in order to increase the reliability and predictability of the seismicity.

In the overall approach, each fault system is divided into a series of segments of equal seismicity. Within each segment, earthquakes are assumed to occur at random as a Poisson process. The distribution of these events, with respect to magnitude, is consistent with a truncated exponential distribution. Fault rupture is taken into account through an empirical relationship between magnitude and fault length which is presented below. The random occurrence of all events from all fault segments, when combined with an attenuation model, is used to develop a probability distribution of peak acceleration at the site. The next section presents a theoretical development of the earthquake occurrence model used in the analysis. The following section describes how the contributions to the seismic hazard from several distinct source regions are combined. Finally, the last section presents the application of these models to the SNM facility.

3.1 EARTHQUAKE OCCURRENCE MODEL

The basic input parameters of the earthquake occurrence model are the magnitude range (upper and lower bound magnitudes) and earthquake recurrence. With respect to earthquake data, the magnitudes are discretized every 1/4 of a magnitude unit as is commonly done in data recording. This representation permits the use of discrete models.

The development of the model involves three steps:

(1) Assuming that earthquake occurrences form a Poisson process with mean rate of occurrence independent of magnitude, a distribution is obtained on the number of occurrences for the time period considered.

(2) Given that an event has occurred, a distribution on the magnitude of events is determined. The process generating model can be assumed to be Bernoulli. The probability of success, p_{M_i}, corresponding to each trial, is defined as the probability that the event that has occurred is of magnitude M_i. Thus, the probability of failure, $q_{M_i} = 1 - p_{M_i}$, at each trial is the probability that the event is not of magnitude M_i. The probability of having r events of magnitude M_i, given that a total of n events have occurred, can therefore be obtained using the binomial distribution.

(3) The distribution of the number of events of each magnitude, independent of the number of trials, is obtained by combining steps one and two.

The present model (nonparametric independent with marginal beta distribution) and more classical parametric model essentially bound more realistic (but more complicated) nonparametric dependent models. Similarity in the results gives

confidence in the present procedure. The present nonparametric model has the advantage of being able to represent nonexponential frequency-magnitude relationships at no extra cost of analysis.

We recognize that, in addition, there are many other models, in various stages of development, that might be applied to the earthquake occurrence model. These include Markov models and models based upon Renewal Theory. We select the models described above based solely on their common usage in earthquake hazard analysis. We qualitatively attempt to account for model uncertainty in a robust sensitivity study on the input variables.

Earthquake Occurrence (Poisson Model)

It is assumed, once the seismic sources have been located, that earthquake occurrences on each source form a Poisson process with mean rate of occurrence independent of magnitude. For earthquake events to follow the Poisson model, the following assumptions must be valid:

1. Earthquakes are spatially independent
2. Earthquakes are temporally independent
3. The probability that two seismic events will take place at the same time and at the same location approaches zero.

The first assumption implies that the occurrence or absence of a seismic event at one site does not affect the occurrence or absence of another seismic event at some other site or the same site. The second assumption implies that seismic events do not have memory. The assumptions of spatial and temporal independence have been verified by data when aftershock sequences are removed, and are commonly accepted. The degree of dependence between events, due to the dual mechanism of stress accumulation and release, has not yet been determined with any amount of precision, but the earth's "memory" appears to fade quite rapidly with time (Garner and Knopoff, 1974). The third assumption implies that, for a small time-interval, more than one seismic event cannot occur on one source.

Thus, considering all the events of magnitude greater than an arbitrary lower bound, a distribution is obtained for the number of occurrences in a given period of time, t. The lower bound is chosen so that earthquakes of magnitude smaller than the one specified, which have a negligible damage potential, can thus be disregarded. This distribution is obtained for each seismic source.

In its general form, the Poisson law can be written as

$$P_N(n/\lambda) = e^{-\lambda t} \frac{(\lambda t)^n}{n!} \quad , \quad t>0 \; ; \; n \text{ integer} \geq 0, \tag{3-1}$$

where

$P_N(n/\lambda)$ = probability of having n events in time period t, given λ
n = number of events
λ = mean rate of occurrence per unit of time

Thus, if the mean rate of occurrence λ is known, the probability distribution function can be defined completely.

The parameter λ is obtained from the data and can be modified subjectively. In the present case, it is expressed as the mean rate of occurrence, per year, of earthquakes larger than magnitude 3.5. Using Equation 3-1, the probability of any number of events within a source region during the future time period can be obtained. As an example:

$$P(0) = \frac{e^{-\lambda t}(\lambda t)^0}{0!} = e^{-\lambda t} \tag{3-2}$$

$$P(1) = e^{-\lambda t} \lambda t, \quad \text{etc.}$$

Since these outcomes are exhaustive and mutually exclusive, the condition $\sum_{n=0} P(n) = 1.0$ is satisfied. Two typical plots of these discrete distributions are given in Figure 3-1.

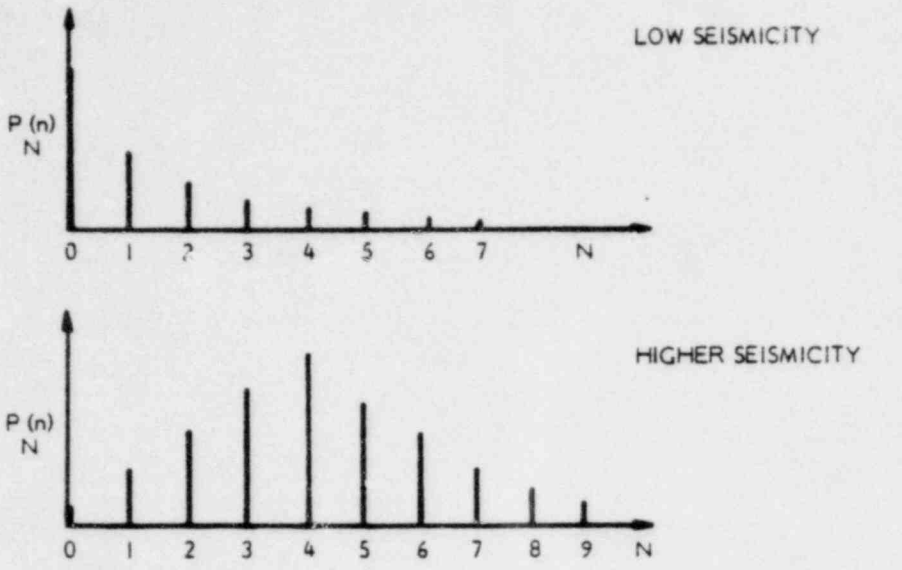

(b) POISSON MODEL - TWO DISCRETE DISTRIBUTIONS FOR N

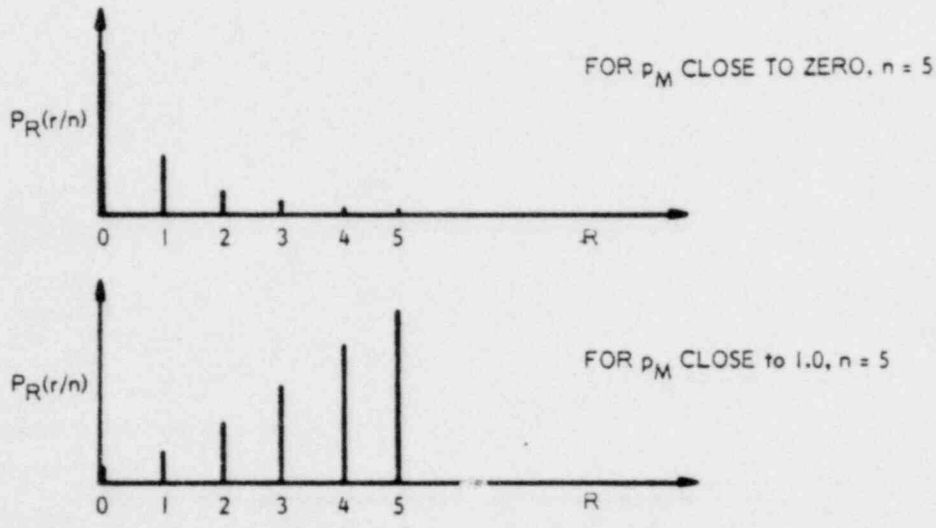

(a) BERNOULLI MODEL - DISCRETE PROBABILITY DISTRIBUTIONS FOR R

FIGURE 3-1

TYPICAL DISTRIBUTIONS FOR POISSON AND BERNOUILLI MODEL

TERA CORPORATION

Estimate of λ

If one assumes that the number of seismic events for a future time t follows a Poisson probability law, there is still uncertainty about the parameter λ, the mean rate of occurrence (Equation 3-1). Therefore, λ is treated as a random variable. The probabilistic information on λ can be obtained through historical data or from the subjective knowledge of the analyst. The subjective probability distribution on λ is called the "prior distribution."

The concept of conjugate prior is used for analytical simplicity (Raiffa and Schlaifer, 1961). Therefore, the prior distribution for the random variable λ is chosen as the gamma distribution with parameters λ' and ν'. Since the gamma distribution can fit a large variety of shapes, this choice does not introduce any major limitations in the model.

Using the historical information, one can obtain the sample likelihood function for λ. The posterior distribution for λ can be obtained by combining the prior distribution and the sample likelihood function by means of Bayes' theorem.

Let $f'_{\Lambda}(\lambda)$ be the prior probability distribution function for λ, and $L(\lambda)$ be the sample likelihood function for λ (given by the Poisson law for n observations), then the posterior distribution $f''_{\Lambda}(\lambda)$ is obtained as

$$f''_{\Lambda}(\lambda) = N_1 L(\lambda) f'_{\Lambda}(\lambda), \tag{3-3}$$

where N_1 is a normalizing constant. The posterior distribution of λ is also gamma type with parameters $\lambda'' = \lambda' + T$ and $\nu'' = \nu' + N$. The parameters T and N are directly available from the data and the parameters λ' and ν' are obtained directly from the shape of the prior distribution or from their equivalent physical meaning: λ' being interpreted as the equivalent time period over which the analyst bases his subjective input and ν' as the equivalent number of occurrences during this time period.

In Equation 3-1, the conditional probability on the number of events n is based on λ. The unconditional or the marginal distribution on n can be obtained by using Equation 3-1 together with Equation 3-3 and integrating over all λ's. Thus,

$$P_N(n) = \int_0^\infty P_N(n/\lambda) f''_\Lambda(\lambda) d\lambda$$

which leads to

$$P_N(n) = \frac{\Gamma(n + \nu'')}{n!\ (\nu'')} \cdot \frac{t^n\ \lambda''^{\nu''}}{(t + \lambda'')^{n+\nu''}} \qquad (3\text{-}4)$$

for n integer ≥ 0, $\nu'' > 0$, $\lambda'' > 0$, $t > 0$.

Equation 3-4 is called the "marginal Bayesian distribution of n." This distribution, after the uncertainties on the mean rate of occurrence are considered, gives the probability of the number of events above a predetermined lower bound M_ℓ, in time period t.

Distribution of Magnitudes (Bernoulli Model)

A Bernoulli trial is used to model information on magnitudes. Given that an event has occurred, the probability that it is of any given Richter magnitude can be represented in terms of a Bernoulli trial. If the seismic event that has occurred is of the M_i under consideration, then the outcome of the Bernoulli trial is a success. Conversely, failure at each trial implies that the seismic event that has occurred is of some other magnitude.

If p_{M_i} = probability of success at each trial corresponding to M_i

and $q_{M_i} = 1 - p_{M_i}$

= probability of failure at each trial,

then using the binomial law,

$$P_R(r_{M_i}/n, p_{M_i}) = C_n^{r_{M_i}} \, p_{M_i}^{r_{M_i}} (1-p_{M_i})^{n-r_{M_i}} \qquad (3\text{-}5)$$

for an integer > 0, r_{M_i} integer; $0 \leq r_{M_i} \leq n$, and $0 \leq p_{M_i} \leq 1$.

where $P_R(r_{M_i}/n, p_{M_i})$ is read as the probability that r_{M_i} events of magnitude M_i will occur out of a total of n events, given that the probability of occurrence of M_i is p_{M_i} at each trial, and

$$C_n^{r_{M_i}} = \frac{n!}{r_{M_i}!(n - r_{M_i})!}$$

A different probability p_{M_i} is obtained for each M_i considered in the model. A similar equation is thus obtained for each of the other magnitudes. The probabilities p_{M_i} are mutually exclusive within the range of selected magnitudes, hence,

$$\sum_{\text{all } M_i} p_{M_i} = 1.0.$$

As an example, for $M_i = 6$ and $n = 5$,

P (0 events of M = 6 given 5 earthquakes) = $(1 - p_6)^5$

P (1 events of M = 6 given 5 earthquakes) = $5 \times p_6 \times (1 - p)^4$

P (5 events of M = 6 given 5 earthquakes) = p_6^5 .

It should be noted that

$$\sum_{r=0}^{n} p(r/n) = 1.0 .$$

Typical plots of the above distribution are shown in Figure 3-1.

Similar plots showing multinomial distribution of different M_i can be obtained as well. They are not of direct interest in the analysis since each M_i is treated separately.

As mentioned at the beginning of this section, the present nonparametric model gives essentially the same results as parametric ones. It is simply more versatile as it can accommodate for nonexponential frequency-magnitude relationship. However, in this study, the well known Gutenberg-Richter earthquake recurrence relationship is adopted and the probability p_{M_i} should be consistent with an exponential distribution of magnitudes. Cornell (1971) has proposed such a distribution which incorporates both lower and upper bound limits on magnitude:

$$P(M \leq m) = K\left\{1 - \text{Exp}\left[-\beta(m - M_{\ell o})\right]\right\} \tag{3-6}$$

where,

$P(M \leq m)$ = probability of $M \leq m$

$K = \left\{1 - \text{Exp}\left[-\beta(M_u - M_\ell)\right]\right\}^{-1}$

$= 2.3b$

M_u = upper bound magnitude

M_ℓ = lower bound magnitude

The probability that an earthquake has a magnitude within the range $m_i \pm \Delta m/2$, equivalent to the Bernoulli parameter p_{M_i}, then becomes

$$p_{M_i} = P(M \leq m_i + \Delta m/2) - P(M \leq m_i - \Delta m/2) \tag{3-7}$$

Equation 3-5 represents the generating process for the number of events M_i. However, this information is conditional on the knowledge about p_{M_i}, the probability of success corresponding to M_i.

Estimate of p_{M_i}

The conjugate prior distribution on p_{M_i}, $f'_P(p_{M_i})$, is assumed to be beta type with parameters η' and ξ'. Since the normalized beta distribution is bounded between 0 and 1, and fits a large variety of shapes, this choice does not introduce any major limitations in the model. A prior distribution of a similar form has to be assumed for each of the magnitudes considered.

The usual format of the available data indicates that, among the n earthquakes observed for a given source, r_{M_i} were of M_i. This information is used in the construction of the sample likelihood function. The sample likelihood function on p_{M_i}, $L(p_{M_i}/n, r_{M_i})$, may be obtained from the generating process (Equation 3-5).

The posterior distribution $f''_P(p_{M_i})$ is given by

$$f''_P(p_{M_i}) = N_1 L(p_{M_i}/n, r_{M_i}) f'_P(p_{M_i}) \tag{3-8}$$

where N_1 is a normalizing constant. The posterior distribution on p_{M_i} is also beta type with parameters η'' and ξ''.

In Equation 3-5, the conditional probability on the number of successes, r_{M_i}, is based on p_{M_i} and n. The condition on p_{M_i} can be removed using Equation 3-8 and integrating over all the values of p_{M_i} as follows:

$$P_R(r_{M_i}/n) = \int_0^1 P_R(r_{M_i}/p_{M_i}, n) f_P''(P_{M_i}) dp_{M_i} \tag{3-9}$$

$$= C_n^{r_{M_i}} \left[\frac{\Gamma(\eta''_{M_i})}{\Gamma(\xi''_{M_i})\Gamma(\eta''_{M_i} - \xi''_{M_i})} \cdot \frac{(\alpha_{M_i})(\beta_{M_i} - \alpha_{M_i})}{\Gamma(\beta_{M_i})} \right]$$

for n integer > 0, r_{M_i} integer; $0 \leq r_{M_i} \leq n$,

$$\text{and} \quad \xi''_{M_i} = \xi'_{M_i} + r_{M_i}$$

$$\eta''_{M_i} = \eta'_{M_i} + n$$

$$r_{M_i} + \xi''_{M_i} = \alpha_{M_i}$$

$$n + \eta''_{M_i} = \beta_{M_i}$$

The parameters r_{m_i} and n are directly available from the data while the parameters M'_{M_i} and ξ_{M_i} are obtaind directly from the shape of the prior distribution or from their equivalet physical meaning: M'_{M_i} being the equivalent number of trials on which the expert bases his subjective input and ξ_{M_i} the equivalent number of successes.

The above expression is the distribution on the number of earthquakes of magnitude M_i given that n earthquakes have occurred. There is a similar distribution for each M_i considered.

Marginal Distribution on the Number of Magnitudes

The distribution of the number of events of each magnitude independent of the number of trials, is obtained from Equations 3-4 and 3-9, thus

$$P_R(r_{M_i}) = \sum_{n=0}^{\infty} P_R(r_{M_i}/n) p_N(n) \qquad (3\text{-}10)$$

$$= \sum_{n=0}^{\infty} C_n^{r_{M_i}} \frac{\Gamma(\eta''_{M_i})}{\Gamma(\xi''_{M_i})\,\Gamma(\eta''_{M_i} - \xi''_{M_i})}$$

$$\cdot \frac{\Gamma(r_{M_i} + \xi''_{M_i})\,\Gamma(n + \eta''_{M_i} - r_{M_i} - \xi''_{M_i})}{(n + \eta''_{M_i})}$$

$$\cdot \frac{\Gamma(n + \nu'')t^n \lambda''^{\nu''}}{n!\,\Gamma(\nu'')(t + \lambda'')^{n + \nu''}}$$

This distribution describes totally the seismicity of the source considered in terms of the two parameters magnitude (M_i) and number of occurrences (n).

The Bernoulli model has the advantage that the probability of occurrence of an earthquake of any given magnitude (p_{M_i}) can be established and updated independently of other magnitudes. It also offers greater flexibility in the use of historical seismicity data and in combining it with subjective information through a Bayesian approach.

3.2 SEISMIC EXPOSURE EVALUATION

A typical seismic region contains a number of earthquake sources. The seismic exposure evaluation aims at combining the effect of all sources to provide an estimate of the probability of occurrence of at least one event of a given ground motion within the time period of interest. By repeating the process for a number of ground motion levels, a probability distribution function or cumulative distribution function for the ground motion is developed at the site.

One of the important elements of a seismic exposure evaluation is the attenuation relation, or transfer function, that specifies the ground motion parameter at the site, given the occurrence of an earthquake. As is conventional in most seismic hazard analyses, we chose to characterize the vibratory motion at the site in terms of peak ground acceleration (PGA). Because of the proximity of the site to the Verona Fault, an attenuation relation that focused on the near-source environment was used. Furthermore, the attenuation relation emphasized the response of embedded structures since the results are to be applied to the response of the SNM facility RML cells, massive thick walled rooms whose outside walls are either partially or totally covered by soil.

The model, which has been previously derived and reported upon (Campbell, 1979), is based on 439 earthquake accelerations from 86 earthquakes recorded within 25 kilometers of the source. The details of this model are presented in Appendix A. A significant fraction of the data was recorded from small earthquakes in the basements of small buildings, thereby permitting a statistical representation of embedment effects. Besides addressing embedment, the statistical analysis of these data also addressed obvious biases contained in the data set, such as multiple recordings from single earthquakes, and the abundance of data from smaller earthquakes. This was dealt with through a weighting scheme in the regression analysis that resulted in each earthquake having the same weight and in each magnitude interval having the same weight. The weighted regression analysis on these data resulted in the following expression for the PGA representative of embedded structures.

$$\text{Ln PGA} = -5.06 + 0.69\, M_L - 0.40\, \text{Ln}\,(R + 1) + (0.016\, M_L - 0.13)\, \text{Ln}^2\,(R + 1)$$

for PGA in g's, R in kilometers, and M_L as local magnitude, with a standard error of estimate of 0.61 and a correlation coefficient of 0.75. This expression is plotted in Figure 3-2.

As discussed above, maximum peak horizontal acceleration (PGA) is the ground motion parameter of interest in this study. In this model the magnitude and PGA are discretized to equal step-increments so that all the integration signs can be replaced by summations. Since the distance is a parameter in the attenuation relationships, the process of dividing a source of length L_o into smaller segments enables one to take into consideration the distance variation to the site from different parts of a long source. The size of the segments is chosen small enough that the approximation from a continuous to discrete computation is acceptable. The seismicity within a source remains the same from segment to segment. From the Gamma distribution, the posterior mean rate of occurrence of earthquakes for a source is ν'' / λ''. The rate for a segment ΔL then becomes

$$\left(\frac{\nu''}{\lambda''}\right)_{\Delta} = \frac{\nu''}{\lambda''} \frac{\Delta L}{L_o} \qquad (3\text{-}11)$$

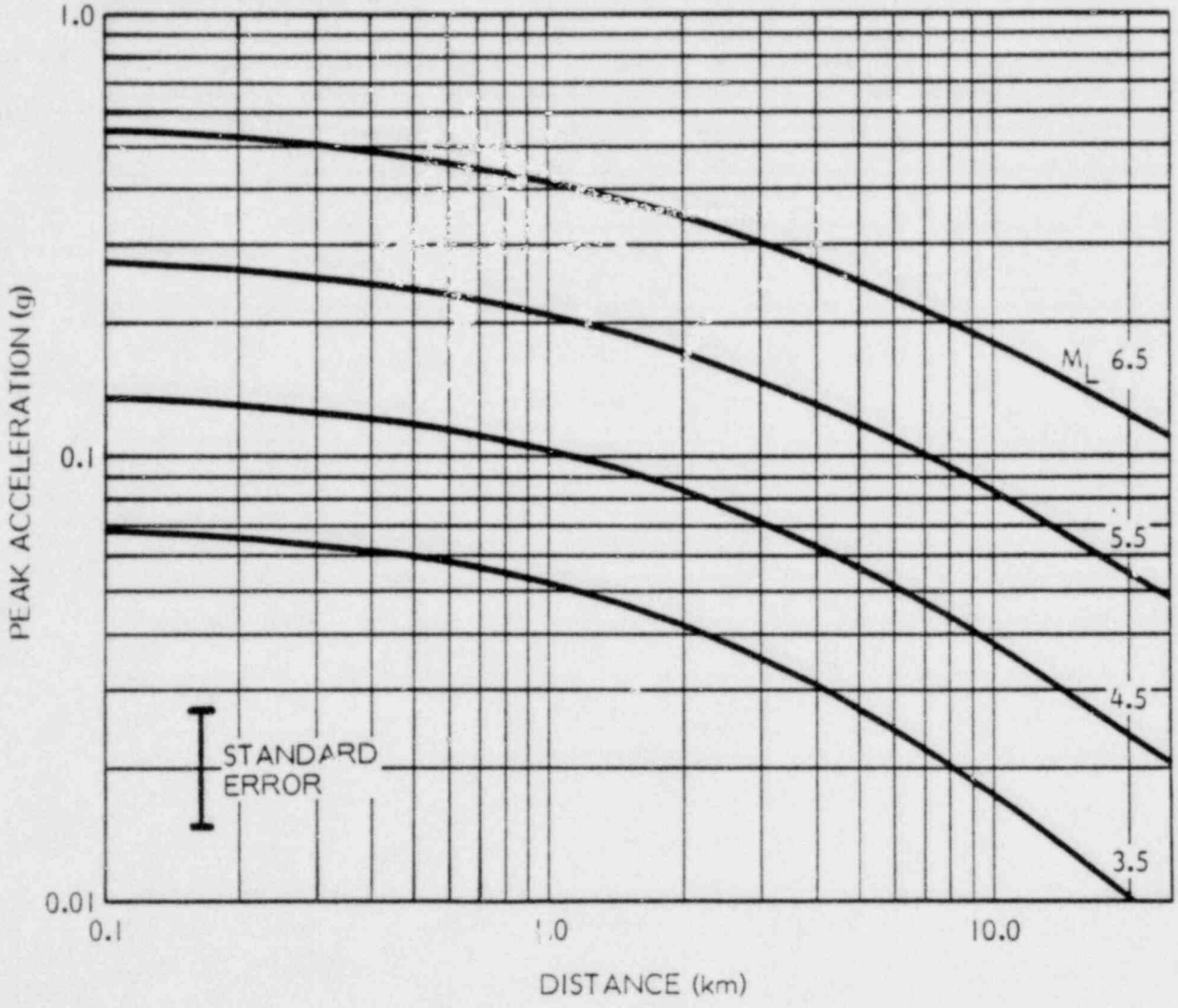

FIGURE 3-2

NEAR SOURCE ATTENUATION OF PEAK HORIZONTAL ACCELERATION FOR EMBEDDED STRUCTURES

The distribution on the number of events for each segment may then be obtained from Equation 3-4, where ν" is replaced by ν_Δ". The conditional distribution on magnitudes, given n events, remains unchanged by the segmentation of the sources. The distribution of the number of occurrences of each magnitude is given by Equation 3-9. The same distribution applies for any segment of the source. The distribution of the number of occurrences of each M increment can be presented under a matrix form that describes the total seismicity of the segment.

Only a finite number of different magnitude events can occur on the segment (from the largest to the smallest magnitude considered). The number of occurrences of any of these events is limited by the associated probability of their occurrence. Events are disregarded when this probability becomes negligible, for example, 10^{-8}. Hence, the total number of events is finite and can easily be handled under the summation signs.

Distances were computed from the location of the closest expected rupture. This was determined by assuming that the hypocenter occuring at the midpoint of a segment will rupture adjacent segments bilaterally, where the length is computed from a relationship between fault length L and magnitude,

$$L(M) = A_L + B_L M. \qquad (3\text{-}12)$$

The rupture width (measured along the dip of the fault) was assumed to be equal to the fault rupture length. Fault lengths were computed as surface length or twice the source radius, whichever was larger.

A description of the fault-length relationship used in the analyses appears in Section 4.0.

Once the distance from the segment to the site is known, all the parameters of the attenuation relationships are determined. For a given event M_j occurring on a segment of distance R_i from the site, the probability of obtaining a maximum

acceleration a_i at the site is given by $f(a_i/M_j,R_l)$, which is the distribution of accelerations for a given magnitude and distance. This distribution is chosen to be lognormal, and reflects the uncertainty in the peak acceleration attenuation relationship.

Contribution of One Segment

The contribution to acceleration greater than or equal to a_i of all events M_j occurring on the same segment is computed as:

$$P(A \geq a_i) = pP(M_j) + \left[1 - (1 - p)^2\right] P(2M_j) + \ldots + \left[1 - (1 - p)^n\right] P(nM_j) \qquad (3\text{-}13)$$

where

$P(A \geq a_i)$ = probability of obtaining acceleration greater than or equal to a_i at least once

$P(kM_j)$ = probability of k occurrences of event M_j with $k = 1, 2 \ldots n$

p = $P(A \geq a_i/M_j)$, probability of obtaining an acceleration greater or equal to a_i given an event M_j.

Setting $q = 1 - p$, the above expression can be rewritten:

$$P(A \quad a_i) = P(\text{no } M_j) + \sum_{k=1}^{n-1} q^k \, P(kM_j) \qquad (3\text{-}14)$$

with n chosen so that $q^n P(nM_j)$ can be neglected.

The above discussion assumes independence among events. Hence, the contribution of all possible events can be combined as follows:

$$P(A \geq a_i)_{\text{one segment}} = 1 - \prod_{\substack{\text{all} \\ M_j}} \left[1 - P(A \geq a_i)_{M_j} \right] \qquad (3\text{-}15)$$

The whole range of magnitudes is included, from the largest one down to the smallest one that generates a noticeable effect at the site ($M_j \geq M_{min}$ as a function of distance). This eliminates the consideration of a large number of events.

Contribution of One or Several Sources

Because the events are assumed to be independent from segment to segment, the contribution of each segment of a source is combined as in Equation 3-15.

$$P(A \geq a_i)_{\text{one source}} = 1 - \prod_{\substack{\text{all} \\ \text{segments}}} \left[1 - P(A \geq a_i)_{\text{one segment}} \right] \qquad (3\text{-}16)$$

When several sources are considered, the same principle is applied for each source. Thus,

$$P(A \geq a_i) = 1 - \prod_{\substack{\text{all} \\ \text{sources}}} \left[1 - P(A \geq a_i) \Big|_{\text{one source}} \right] \qquad (3\text{-}17)$$

This expression gives the probability that, at least once during the period of interest a_i will be exceeded.

Once a cumulative distribution function is established for a site, the seismic exposure can be determined for any desired probability of nonexceedence.

It has become customary to qualify a load in terms of return period rather than in terms of probability of exceedence. We feel that return period is a bad surrogate for probability as its use may induce confusion. A better approach is to fix the time interval of actual interest (e.g., the next 50 years) and consider various probabilities of exceedence within that time interval. However, to comply with the present trend, we present the concept of return period and its relation to probability. We also present our results in terms of return periods.

Before discussing this process, the following definitions are presented:

PROBABILITY OF NONEXCEEDENCE	The probability that a given level of ground motion will not be exceeded within the period of interest
PERIOD OF INTEREST	The assumed design life or useful life of a structure or project
RETURN PERIOD (RP)	The mean waiting time for an event of interest (assuming a Poisson law of occurrence of earthquakes).

Once a period of interest is selected, the acceleration corresponding to a given probability of nonexceedence or a given return period can be estimated by considering the Poisson character events with site acceleration greater or equal to a_i

The following development assumes no statistical uncertainty on the parameters. More complicated treatment would be needed to take such uncertainty into account.

$$P(A \geq a_i) = 1 - e^{\lambda(a)T}$$

in which

$\lambda(a)$ = mean rate of occurrence of events with site acceleration greater or equal to a_i

T = time period of interest

Thus, if the period of interest is 50 years and an acceleration corresponding to a 200-year return period is desired for a site, we proceed as follows:

$$\lambda(a) = \frac{1}{RP} = \frac{1}{200} = 0.005$$

Hence the probability of non-exceedence in 50 years is

$$\underline{P}(A < a_i) = e^{-0.005 \times 50}$$

$$= 0.779$$

Hence, probability of exceedence in 50 years = 1 - 0.778 ≈ 0.22. The desired acceleration may be found from the CDF corresponding to a probability of exceedence = 22%.

Figure 3-3 gives a relationship between return period, period of interest, and probability of nonexceedence. Note that this shows that accelerations associated with a 200-year return period have a 22% probability of being exceeded in 50 years. The relationship is general and can be applied to any situation based on the Poisson's law for mean rate of occurrence.

The following observations are useful with regard to the return period concept.

(i) A return period (RP) is the mean (or average) waiting time for an event of interest (assuming Poisson occurrence of events).

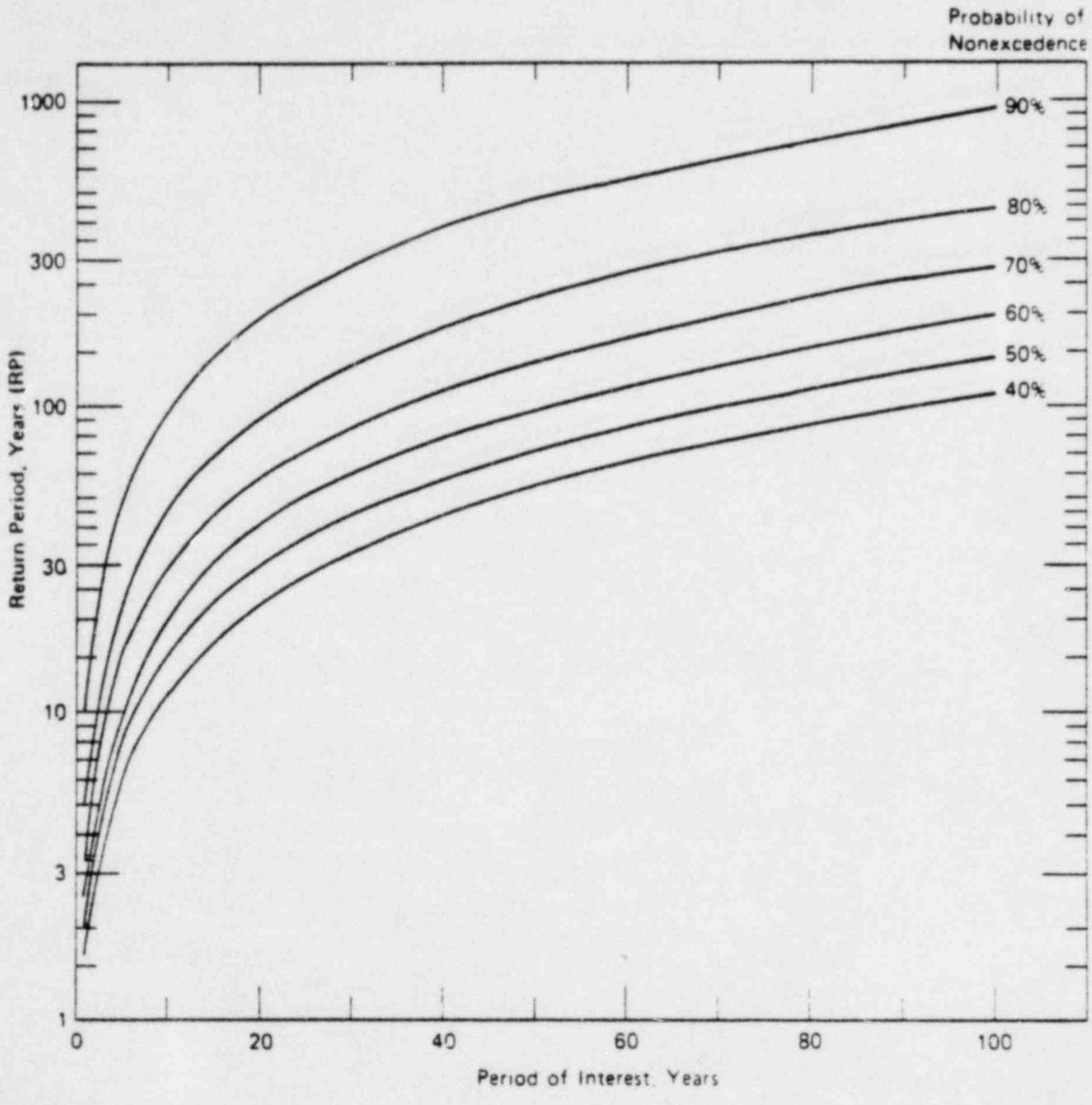

FIGURE 3-3

RELATIONSHIPS BETWEEN RETURN PERIOD, PERIOD OF INTEREST AND PROBABILITY OF NONEXCEEDENCE

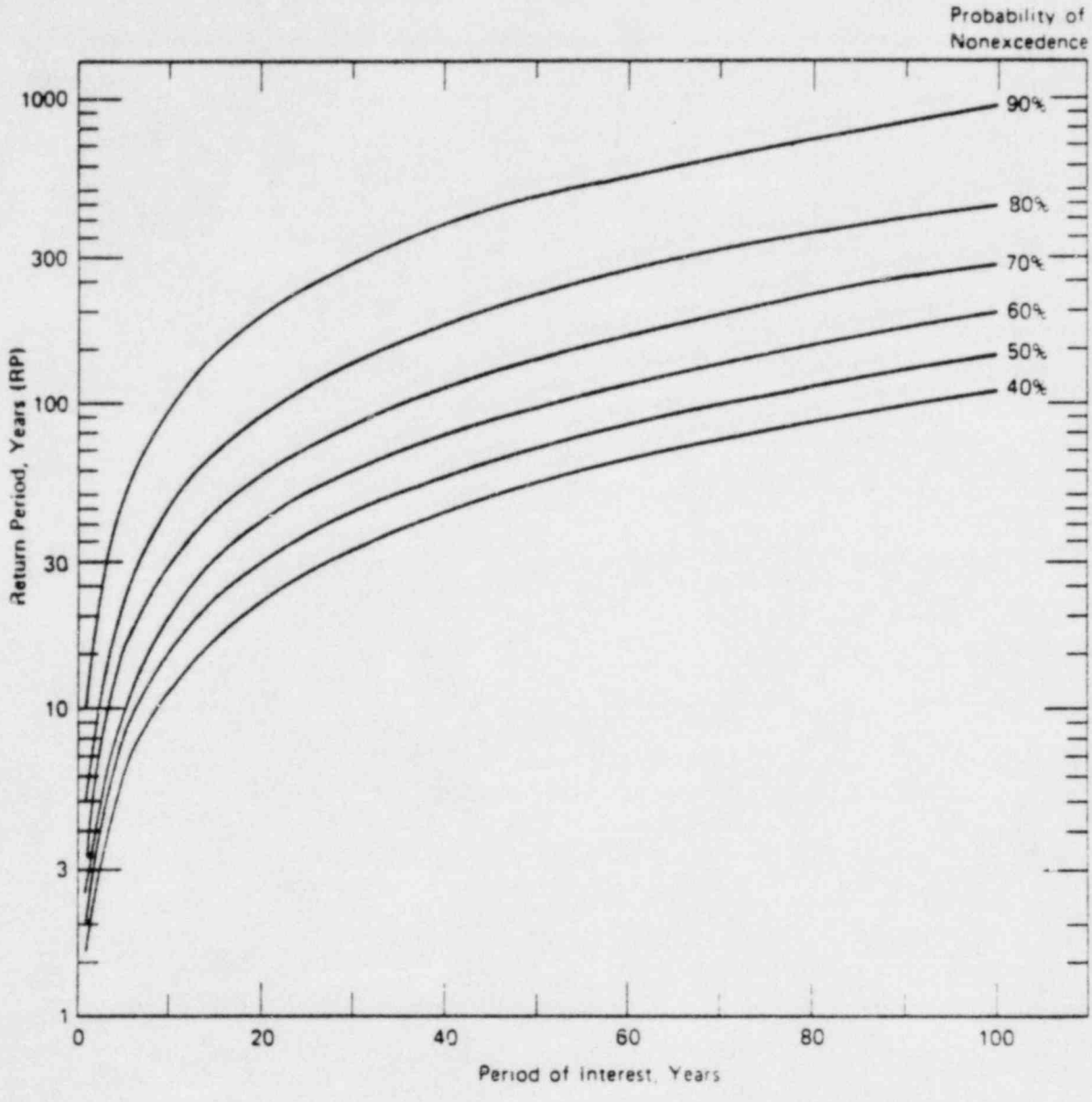

FIGURE 3-3

RELATIONSHIPS BETWEEN RETURN PERIOD,
PERIOD OF INTEREST AND PROBABILITY
OF NONEXCEEDENCE

(2) The probability that an event corresponding to a return period RP will occur in any given year can be approximated by 1/RP. Hence, for a return period of 500 years, $p \approx 0.002$.

(3) The probability that no event of the RP type will occur in RP years is 1/e, where e = 2.718. Thus, if the return period is 100 years, the probability that in 100 years there will not be a single event producing the 100-year peak ground acceleration is given by $1/e \approx 0.36$, or there is a 64% chance that in 100 years there will be at least one event producing a 100-year peak acceleration or more.

3.3 SITE HAZARD RESULTS

The ground motion hazard model presented in the previous sections (in Equations 3-10 through 3-17), was used to establish a distribution for the probability of exceedence of given levels of peak acceleration for the SNM facility. It is very important to note that although the previously described model includes Bayesian elements, these elements were not exercised in this application. In other words, the model was run without any updating of parameters that would ordinarily account for prior subjective probabilities.

A lower bound magnitude of 3.5 was selected to represent a threshold below which earthquake occurrences could be neglected. A best estimate upper bound magnitude of 6.0 was adopted for the Verona Fault based on the geologic data and interpretations in Section 2.0.

The results of the analysis, which are presented in Figure 3-4 for peak horizontal accelerations of 0.1 to 0.8 g, suggest that the occurrence of peak accelerations exceeding 0.3 g and 0.6 g may be associated with return periods of 2,000 and 60,000 years, respectively. Also shown on this figure is our estimate of the plus and minus one standard deviation about this best estimate.

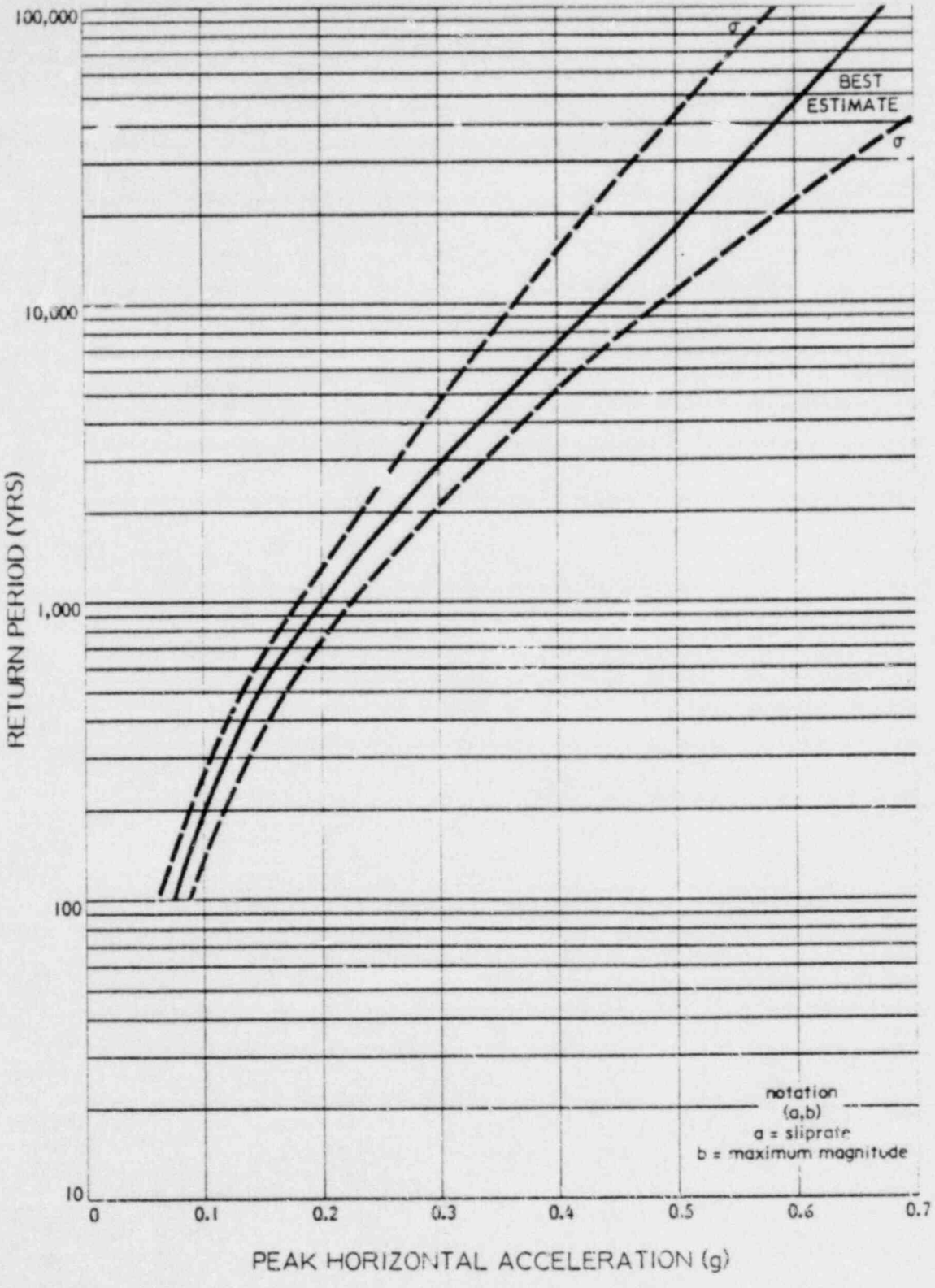

FIGURE 3-4

PEAK ACCELERATION V.S.
RETURN PERIOD FOR THE
SNM FACILITY

4.0 FAULT RUPTURE HAZARD

The proximity of several shears to the SNM facility suggests a possible risk due to fault rupture. A rigorous analysis of this risk would require a detailed knowledge of the fault and fracture pattern in the immediate vicinity of the facility, which is beyond the scope of this study. A general assessment may be made through a study of the fault rupture hazard associated with the adjacent postulated Verona Fault.

Fault rupture hazard is defined as the probability that the maximum surface displacement at a point on the fault exceeds a given value over the time period of interest. The general approach is similar to that used in assessing ground motion hazard (Section 3.0). Each fault system is divided into a series of segments of equal seismicity. Earthquake occurrences within each segment are treated as Poisson-Bernoulli processes, as before. The random occurrence of all events from each fault is combined with a fault rupture model to develop a probability distribution of surface displacement for any point on the fault.

4.1 FAULT RUPTURE PARAMETERS

The three fault rupture parameters required in the development of the hazard model are fault rupture length (L), fault rupture displacement (D), and fault rupture radius (R). Models used to estimate these parameters from earthquake magnitude (M) were developed from regression analyses using the method of least squares. A statistical summary of these analyses is presented in Table 4-1, and tabulated values of the parameters are provided in Table 4-2.

Fault Length (L)

Slemmons (1977) has recently tabulated fault length and displacement data for 87 worldwide earthquakes occurring since 1819. He used these data to develop relationships between magnitude and fault length, where fault length was the independent variable. His equations are thus valid for estimating magnitude from fault length.

TABLE 4-1

SUMMARY OF REGRESSION ANALYSES FOR FAULT LENGTH, FAULT DISPLACEMENT AND SOURCE RADIUS

$$\ln Y = A_Y + B_Y M$$

Parameter	Coefficients		Standard Error	Correlation Coefficient	N
	A_Y	B_Y			
Fault Length, L(km)	-4.670	1.185	0.83	0.76	73
Fault Displacement, D(cm)	-3.797	1.273	0.84	0.76	73
Source Radius, R(km)	-3.391	0.843	0.63	0.73	163

TABLE 4-2

TABULATED VALUES OF FAULT LENGTH,
FAULT DISPLACEMENT, AND SOURCE RADIUS

Magnitude (M_L)	Fault Length L9km)	Source Radius R(km)	Fault Displacement D(cm)
3.5	0.6	0.6	1.9
4.0	1.1	1.0	3.7
4.5	2.0	1.5	6.9
5.0	3.6	2.3	13.0
5.5	6.3	3.5	25.0
6.0	12.0	5.3	47.0
6.5	21.0	8.0	88.0
7.0	38.0	12.0	166.0

In our model, what is required is an estimate of length when magnitude is known. Therefore, the regression analyses were repeated using M as the independent variable. The limited amount of data available on normal-oblique slip faults precluded their exclusive use in the analysis. Therefore, it was decided to use data from all fault types in the regression.

Based on the 73 observations for $4.0 \leq M \leq 8.7$ in Slemmons (1977), the log-linear relationship between L and M was found to be

$$\text{Ln } L(M) = -4.67 + 1.19\ M \qquad (4\text{-}1)$$

for fault length in kilometers.

Fault Displacement (D)

A similar analysis was run for maximum fault displacement. Again using the Slemmons (1977) data for all fault types, the log-linear relationship between D and M was determined as

$$\text{Ln } D(M) = -3.80 + 1.27\ M \qquad (4\text{-}2)$$

for displacement in centimeters.

Source Radius (R)

Source radius is a measure of the true rupture dimensions, not just those observed on the surface after the earthquake. It requires that theoretical source spectrum shapes be fitted to observed spectra, and that the source parameters be estimated from theoretical dislocation models. Source radius thus represents the radius of a circular rupture surface whose area is equivalent to that of the actual rupture surface.

From Brune's (1970) dislocation model, source radius may be computed from the relationship

$$R = \frac{2.34\beta}{2\pi f_o} \qquad (4\text{-}3)$$

where β is the shear-wave velocity of the medium, and f_o is corner frequency (the point where the high frequency decay begins on the source displacement spectrum).

Using this model, Thatcher and Hanks (1973) estimated the source radius of many Southern California earthquakes. Campbell (1977) expanded this set to include 163 earthquakes of $3.0 \leq M_L \leq 6.8$. Using these data, the following log-linear relationship between R (in kilometers) and M was established:

$$\text{Ln } R(M) = -3.39 + 0.84\ M \qquad (4\text{-}4)$$

4.2 FAULT RUPTURE HAZARD MODEL

For an earthquake of given magnitude and location, the probability of observing a displacement greater than a particular level at a point on the fault located at a distance, x_i, is comprised of a joint probability of three events. The first is the probability that surface rupture occurs, which we will designate as "event E_s." The second is the probability that surface rupture extends at least as far as the point of interest (designated as "event E_ℓ"). The last is the probability that the displacement exceeds the specified value (designated as "event E_d").

Mathematically, this joint probability may be expressed as

$$P(D > d \mid M_j, x_i) = P(E_d \cap E_\ell \cap E_s)$$

where M_j is the magnitude under consideration and x_i is the distance along the fault from segment i (the location of the earthquake) to the point in question (Figure 4-1).

Simplifying, by means of conditional probability theory,

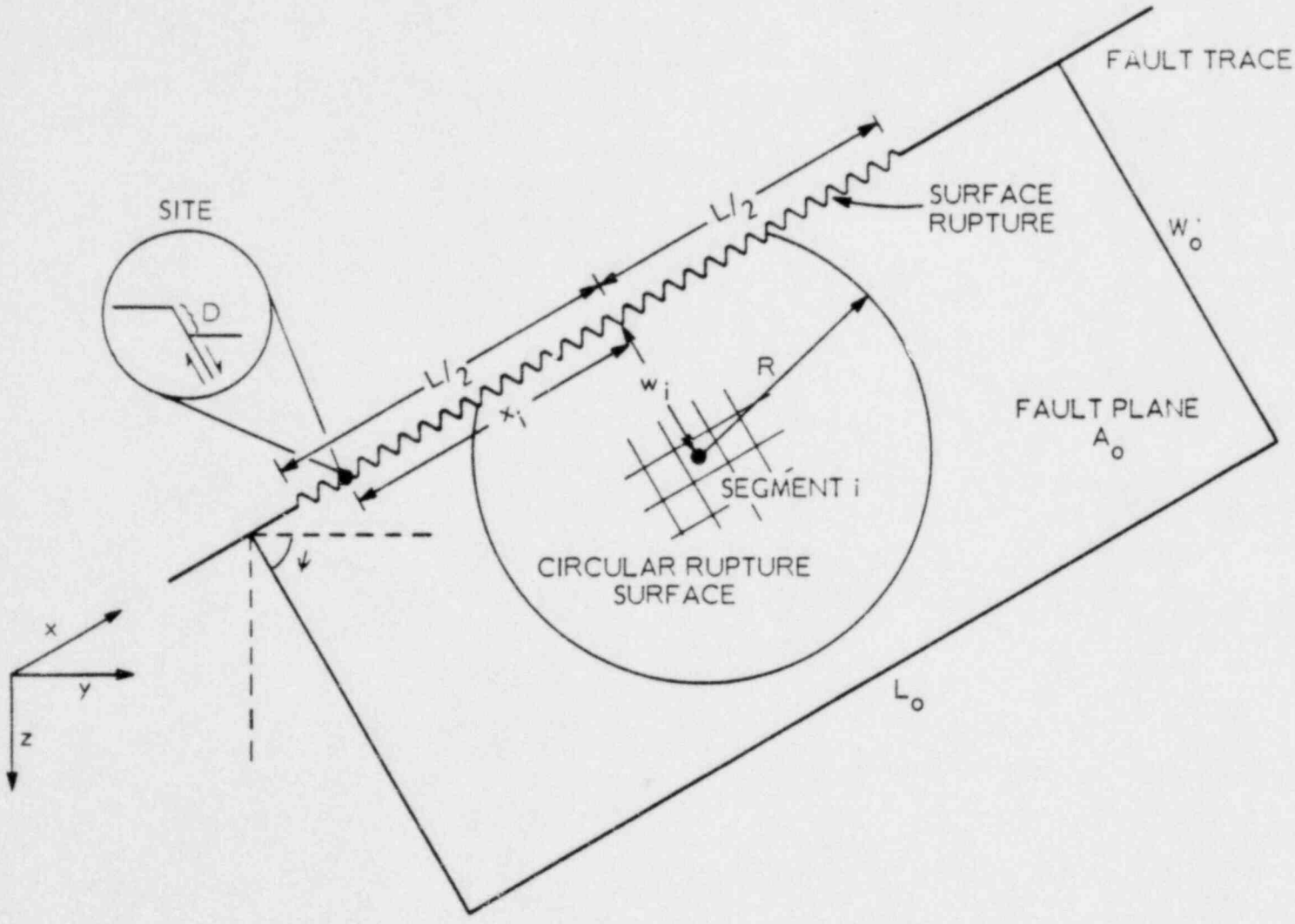

FIGURE 4-1

SCHEMATIC OF THE FAULT RUPTURE HAZARD MODEL

$$P(D > d \mid M_j, x_i) = P(E_d \mid E_\ell \cap E_s) \cdot P(E_\ell \cap E_s)$$

$$= P(E_d \mid E_\ell \cap E_s) \cdot P(E_\ell \mid E_s) \cdot P(E_s) \qquad (4\text{-}5)$$

with all events being contingent upon the occurrence of a given earthquake. After developing models for the above probabilities and unconditionalizing with respect to M_i and x_i, Equation 4-5 may then represent the hazard from all possible earthquakes on the fault.

$\underline{P(E_s)}$

Surface rupture during a given earthquake is assumed to occur if the source radius (R) is greater than the distance along the fault plane from the center of the rupture to the ground surface, designated as "w_i" (Figure 4-1). Since, for a given earthquake, the horizontal extent of faulting tends to be greater than the vertical extent, this definition of surface rupture is considered conservative.

For a given magnitude M_j, we may compute source radius from Equation 4-4),

$$\text{Ln } Rj = A_R + B_R M_j \qquad (4\text{-}6)$$

Because of uncertainty in this expression, Rj may be considered a random variable. Let us assume Rj to be lognormally distributed with a median of Ln Rj and a standard deviation $_R$ (on Ln R) equal to the standard error of estimate, Table 4-1. Then, the probability that Rj is greater than w_i (the event E_s) is given by

$$P(E_s) = P(Rj > w_i)$$

$$= 1 - P(Rj \leq w_i)$$

$$= 1 - \frac{1}{\sigma_R \sqrt{2\pi}} \int_{-\infty}^{\text{Ln } w_i} \text{Exp}\left[-1/2 \left(\frac{y - \text{Ln } R_j}{\sigma_R}\right)^2\right] dy$$

$$= 1 - \Phi\left(\frac{\text{Ln } w_i - \text{Ln } R_j}{\sigma_R}\right) \qquad (4\text{-}7)$$

where Φ (*) represents the standard-normal cumulative distribution function.

$P(E_\ell \mid E_s)$

Given that a surface rupture occurs, let it be assumed that its length is equally distributed in both directions along the fault trace (i.e., bilateral rupture). The midpoint of this rupture is directly above the assumed point of initiation (Figure 4-1). For rupture to occur at the site of interest, it must proceed at least as far as that distance from the midpoint of the surface expression to the site, x_i. Therefore, rupture occurs at the site if $L_j/2 > X_i$, where L_j is the surface rupture length associated with a magnitude M_j event.

L_j is computed from Equation 4-13, thus

$$\text{Ln } L_j = A_L + B_L M_j \qquad (4\text{-}8)$$

To account for uncertainty in the regression, L_j is considered lognormally distributed, with median Ln L_j and standard deviation (on Ln L) of σ_L, equivalent to the standard error of estimate of the regression, Table 4-1.

The probability of the event E_ℓ occurring (given E_r), becomes

$$P(E_\ell \mid E_r) = P(L_j/2 > x_i)$$

$$= P(L_j > 2x_i)$$

$$= 1 - P(L_j \leq 2x_i)$$

$$= 1 - \Phi\left(\frac{\text{Ln } L_j - 2x_i}{\sigma_L}\right) \qquad (4\text{-}9)$$

$\underline{P(E_d \mid E_\ell \cap E_s)}$

Given that surface rupture occurs and that it proceeds at least as far as the site, the surface displacement associated with the earthquake M_j may be estimated from Equation 4-2 as follows:

$$\text{Ln } D_j = A_D + B_D M_j \qquad (4\text{-}10)$$

Accounting for uncertainty in this estimate, D_j is considered lognormally distributed, with median Ln D_j and standard deviation (on Ln D) of σ_D, equivalent to the standard error of estimate of the regression, Table 4-1. The probability that the displacement exceeds some specified value d then becomes

$$P(E_d \mid E_\ell \cap E_s) = P(D_j > d)$$

$$= 1 - P(D_j \leq d)$$

$$= 1 - \Phi\left(\frac{\text{Ln } D_j - \text{Ln } d}{\sigma_D}\right) \qquad (4\text{-}11)$$

Displacement Hazard

The surface displacement hazard for a point on a fault associated with an earthquake on segment i of magnitude M_j is obtained by substituting Equations 4-7, 4-9 and 4-11 into Equation 4-5.

$$P(D > d \mid M_j, x_i) = \left[1 - \Phi\left(\frac{\text{Ln } D_j - \text{Ln } d}{D}\right)\right] \cdot \left[1 - \Phi\left(\frac{\text{Ln } L_j - \text{Ln } x_i}{L}\right)\right] \cdot \left[1 - \Phi\left(\frac{\text{Ln } R_j - \text{Ln } w_i}{R}\right)\right] \quad (4\text{-}12)$$

The total hazard at the point in question requires combining the hazards associated with all possible earthquakes hypothesized to occur on the fault. For this purpose, the two-dimensional fault plane of area A_o is divided into an equal number of segments of equal seismicity.

The development of the surface rupture displacement hazard from this point on is equivalent to the development of the ground motion hazard described in Section 3.2, Equations 3-13 through 3-18. Letting $q = 1 - P(D > d \mid M_j, x_i)$, then, by Equation 3-14,

$$P(D \leq d \mid M_j, x_i) = P(n_o M_j) + \sum_{k=1}^{n} q^k P(kM_j) \quad (4\text{-}13)$$

The contribution of all possible events on segment i becomes

$$P(D > d \mid x_i) = 1 - \prod_{\substack{\text{all} \\ M_j}} \left[1 - P(D > d \mid M_j, x_i)\right] \quad (4\text{-}14)$$

and the contribution of all segments becomes

$$P(D > d) = 1 - \prod_{\substack{\text{all} \\ X_i}} \left[1 - P(D > d \mid x_i)\right] \quad (4\text{-}15)$$

This expression gives the probability of a displacement exceeding d at least once during the exposure period of interest. The associated return period becomes

$$RP = \left\{ 1 - \left[1 - P(D > d) \right]^{1/t} \right\} \qquad (4\text{-}16)$$

where t is the exposure period of interest in years.

4.3 SITE HAZARD RESULTS

The fault rupture hazard associated with the Verona Fault was investigated using the model developed in the previous section, the geologic data presented in Section 2.3, and the earthquake occurrence model developed in Section 3.1. A fault width of 18 km was used in the analysis, consistent with the fault geometry of the Verona fault and an assumed maximum depth of faulting of 15 km. Distributions for the exceedence probabilities of maximum surface displacement were developed for a point on the Verona Fault adjacent to the SNM facility.

The results of the analysis may be found in Figure 4-?. The best estimate return period associated with a maximum displacement exceeding one meter is 19,500 years. The corresponding annual exceedence probabilities is 5×10^{-5}. We also present in this figure our estimate of the plus and minus one standard deviation about this best estimate curve.

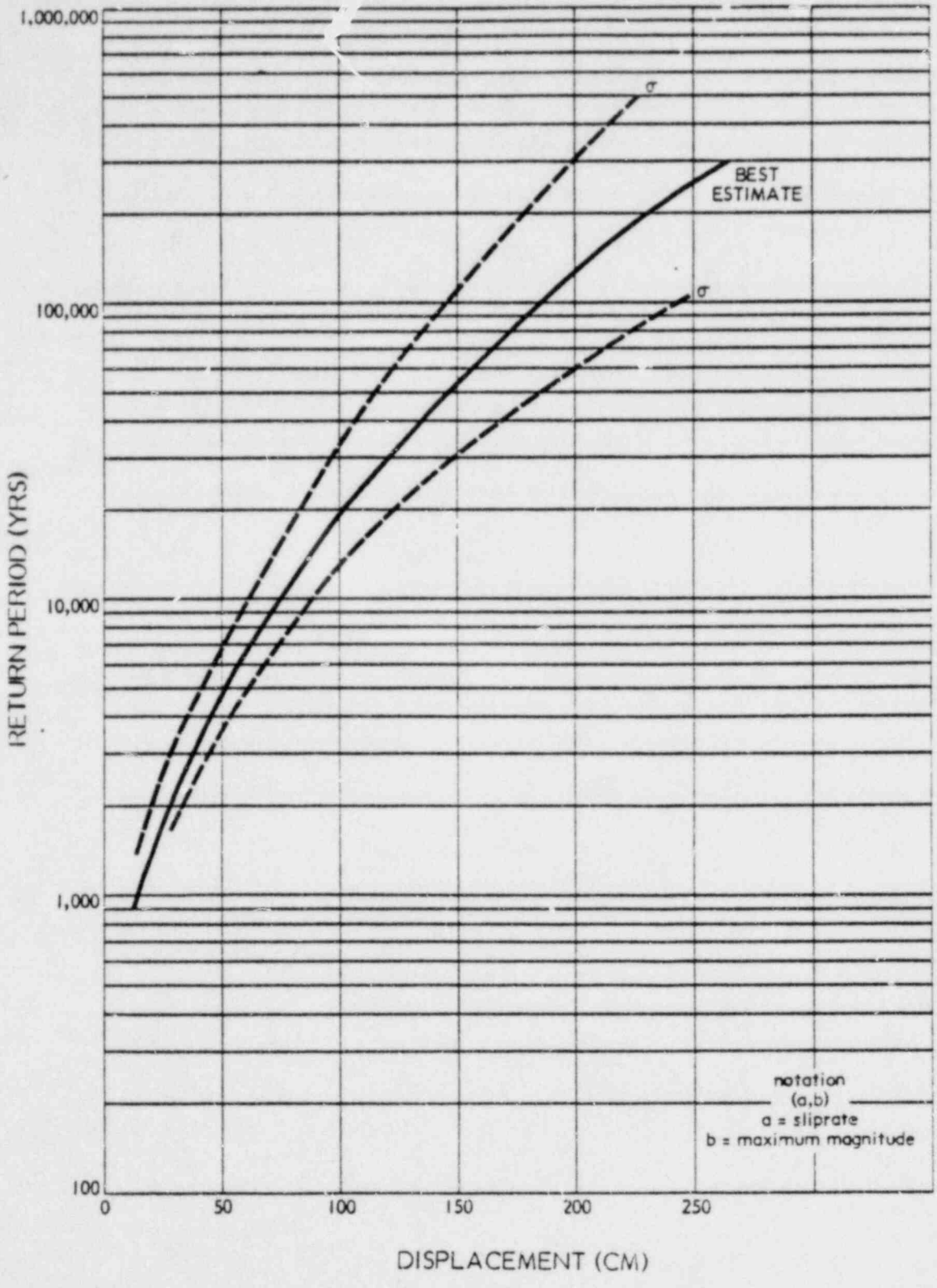

FIGURE 4-2

RUPTURE DISPLACEMENT V.S.
RETURN PERIOD FOR .4E SNM FACILITY

5.0 REFERENCES

Anderson, J. G. (1979). "Estimating the Seismicity from Geological Structure for Seismic Risk Studies," Bull. Seism. Soc. Am., 69(1):135-158.

Bonilla, M. G., and Jane M. Buchanan (1970). "Interim Report Worldwide Historic Surface Faulting," USGS Open-File Report.

Bolt, B. A. and R. D. Miller (1975). Catalogue of Earthquakes in Northern California and Adjoining Areas, January 1, 1910 to December 31, 1972, Seismographic Stations, Univ. of California, Berkeley, California, 1-567.

Brune, J. N. (1968). "Seismic Moment, Seismicity and Slip Rate Along Major Fault Zones," J. Geophys. Res., 73:777-784.

Campbell, K. W. (1977). "The Use of Seismotectonics in the Bayesian Estimation of Seismic Risk," School of Engineering and Applied Science, University of California, Los Angeles, UCLA-ENG-7744.

Campbell (1979). Presentation to the Eastern Section of the Seismological Society of America, Blacksburg, VA.

Cornell, C. A. (1971). "Probabilistic Analysis of Damage to Structures Under Seismic Loads," Dynamic Waves in Civil Engineering, edited by D. A. Howells et al., John Wiley and Sons, London.

Earth Sciences Associates (1978). Geologic Evaluations of GETR Structural Design Criteria, Reports 1: Effects of Earthquake Source and Transmission Path Geology on Strong Ground Motion at GETR Site, Report 2: Ground Motion and Displacement on a Hypothetical Verona Fault, Report 3: Geologic and Seismologic Parameters of Near-Field Strong Motion Records, for General Electric Company. Vallecitos Nuclear Center, Pleasanton, California.

_____ (1978 and 1979). Geologic Investigation, General Electric Test Reactor Site, Vallecitos, California. Prepared for General Electric Company, Phase I and II.

Gardner, J. F., and L. Knopoff (1974). "Is the Sequence of Earthquakes in Southern California, with Aftershocks Removed, Poissonian?," Bull. Seism. Soc. Am., 64:1363-1367.

Greensfelder, R. W. (1972). "Maximum Credible Rock Accelerations in California: Map Sheet 23," California Division of Mines and Geology.

Herd, D. H. (1977). Geologic Map of the Las Positas, Greenville and Verona Faults, Eastern Alameda Co., California. USGS Open-File Report 77-689.

Molnar, P. (1979). "Earthquake Recurrence Intervals and Plate Tectonics," Bull. Seism. Soc. Am., 69(1):115-133.

Raiffa, H., and R. Schaifer (1968). Applied Statistical Decision Theory, Massachusetts Institute of Technology Press, Cambridge.

Slemmons, D. B. (1977). "Faults and Earthquake Magnitude," in State-of-the-Art for Assessing Earthquake Hazards in the United States, U.S. Army Engineers Waterways Experiment Station, Vicksburg, Miss., Misc. Paper S-73-1, Rept. 6.

Thatcher, W., and T. C. Hanks (1973). "Source Parameters of Southern California Earthquakes," J. Geophys. Res., 78:8547-8576.

APPENDIX A

NEAR-SOURCE ATTENUATION

Because of the close proximity of the SNM to the Verona Fault, a model of near-source attenuation of peak horizontal acceleration (PHA) was required. Near-source attenuation models available in the literature have been primarily based upon subjective extrapolations of far-field data, with very few near-source data to support them (e.g., Donovan and Bornstein, 1978; Patwardhan, et al., 1978). Other models are further restricted to a single magnitude (e.g., Seed et al., 1975; Idriss and Power, 1978).

A TERA near-source, strong motion data base was used to develop an attenuation relationship for PHA which is valid for distances less than about 20 km and magnitudes greater than 3.5. This section describes the sources, selection criteria, organization and analysis of these data as applied to this analysis.

A.1 THE DATA BASE

The near-source data base used for this study represents earthquakes which have occurred in the United States, Central America, and Asia. Oroville aftershock data were provided by Hanks (1978). Various sources were used to compile the remaining data, which are generally from the western U.S. Overall, there were 214 near-source records in the Oroville sequence, and 198 in the western U.S.

The data base is organized in three files: an earthquake file, a station file and a strong-motion file. The earthquake data file contains information concerning the event, such as: TERA I.D. number, date, time, latitude, longitude, quality of the location, local Richter magnitude, body-wave magnitude, surface-wave magnitude, epicentral intensity, depth, and event name.

The station data file contains information concerning the site of the strong-motion instrument, such as: USGS station number, latitude, longitude, structure

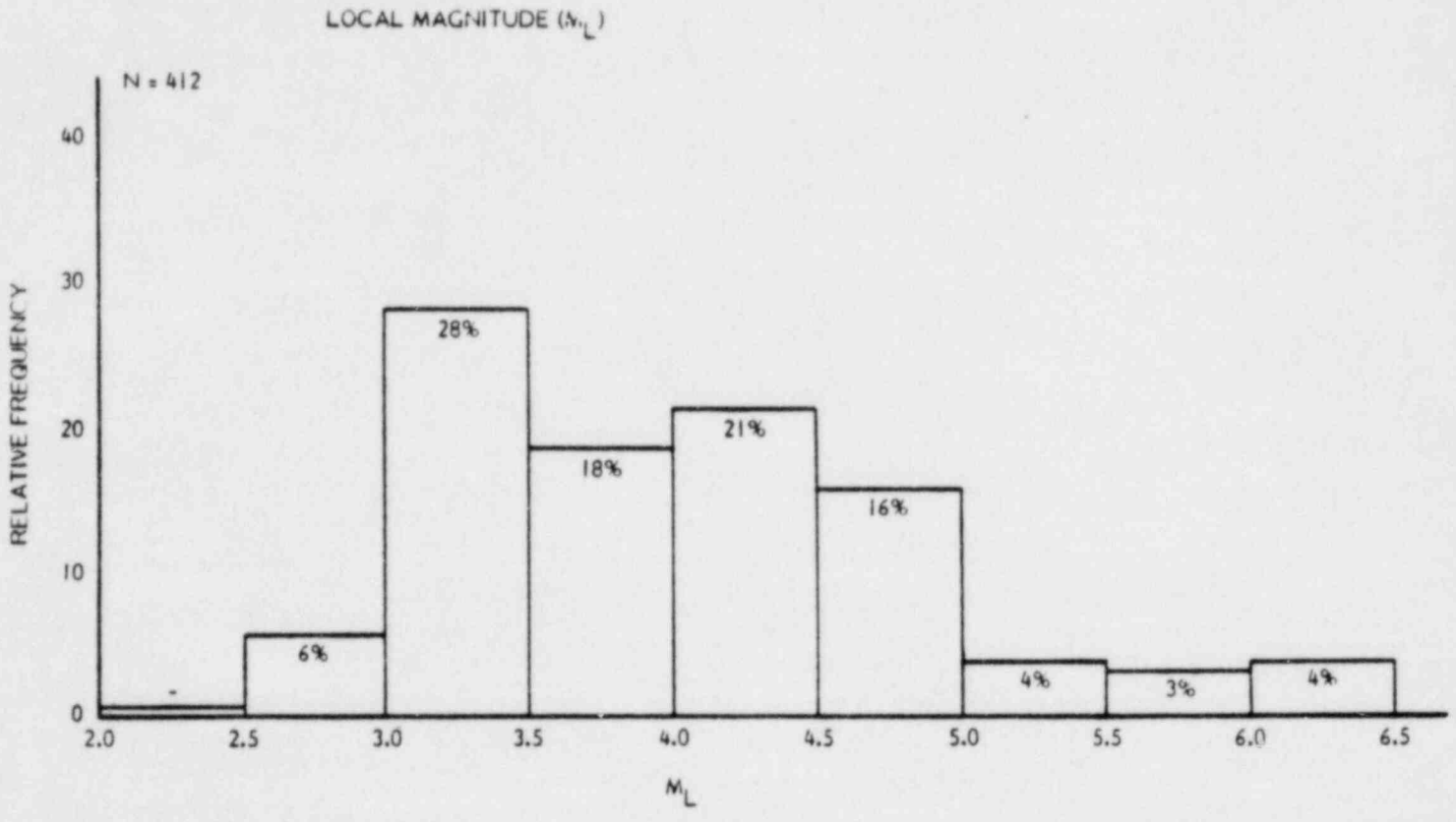

FIGURE A-1

DISTRIBUTION OF MAGNITUDE FOR THE
NEAR SOURCE STRONG MOTION DATA BASE

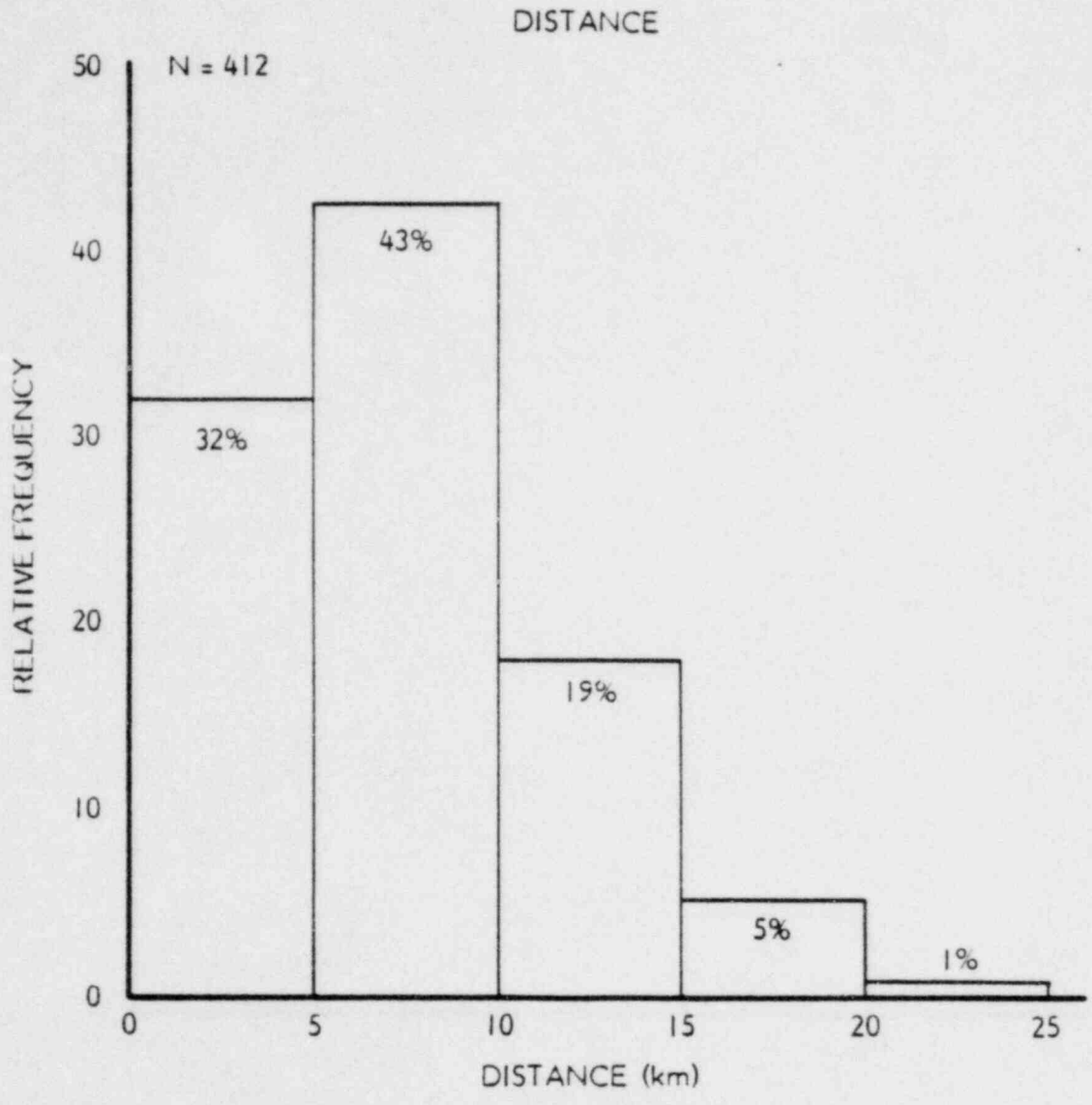

FIGURE A-2

DISTRIBUTION OF DISTANCE FOR THE
NEAR SOURCE STRONG MOTION DATA BASE

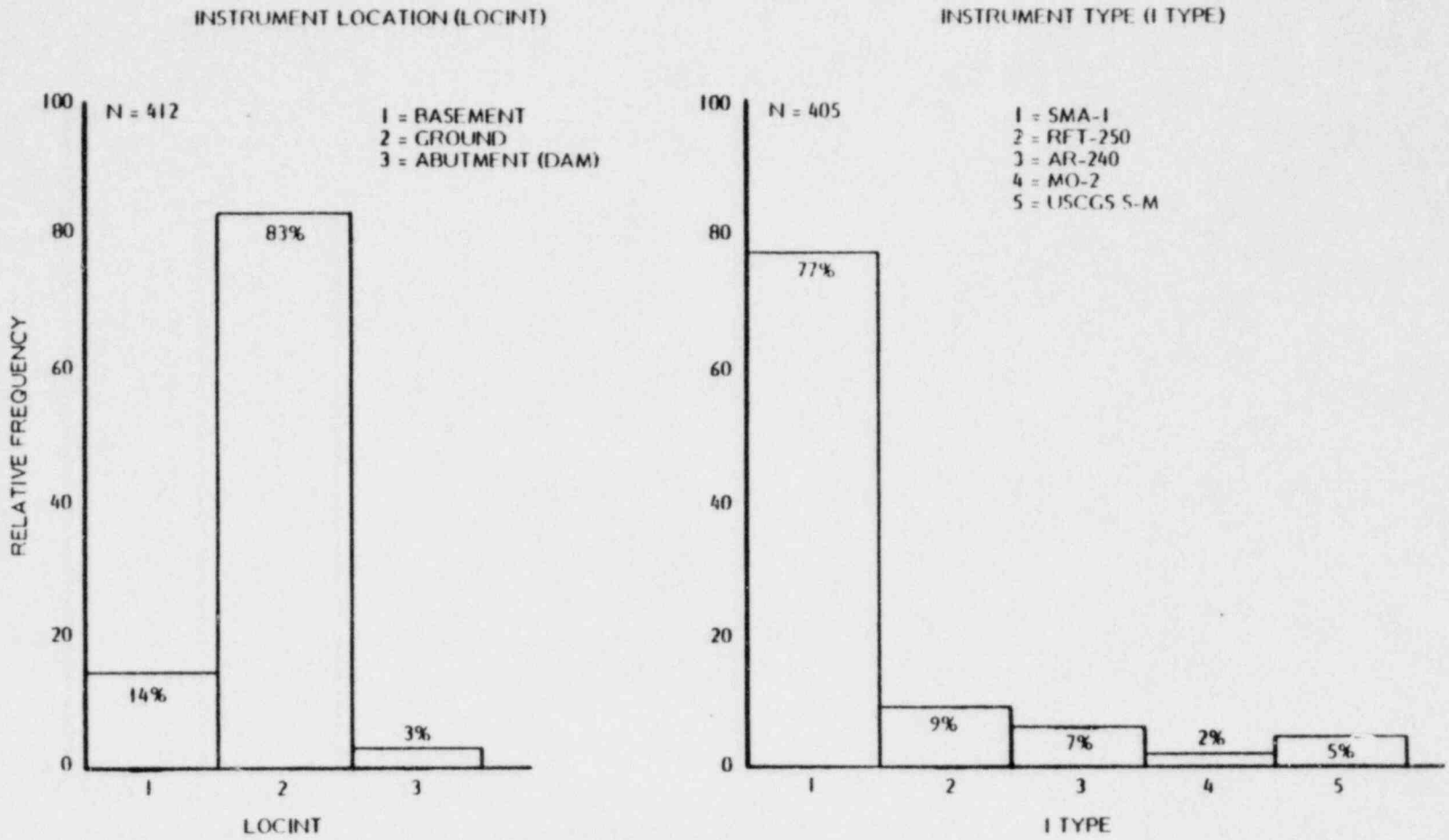

FIGURE A-3

DISTRIBUTION OF RECORDING INSTRUMENT TYPE AND LOCATION
FOR THE NEAR SOURCE STRONG MOTION DATA BASE

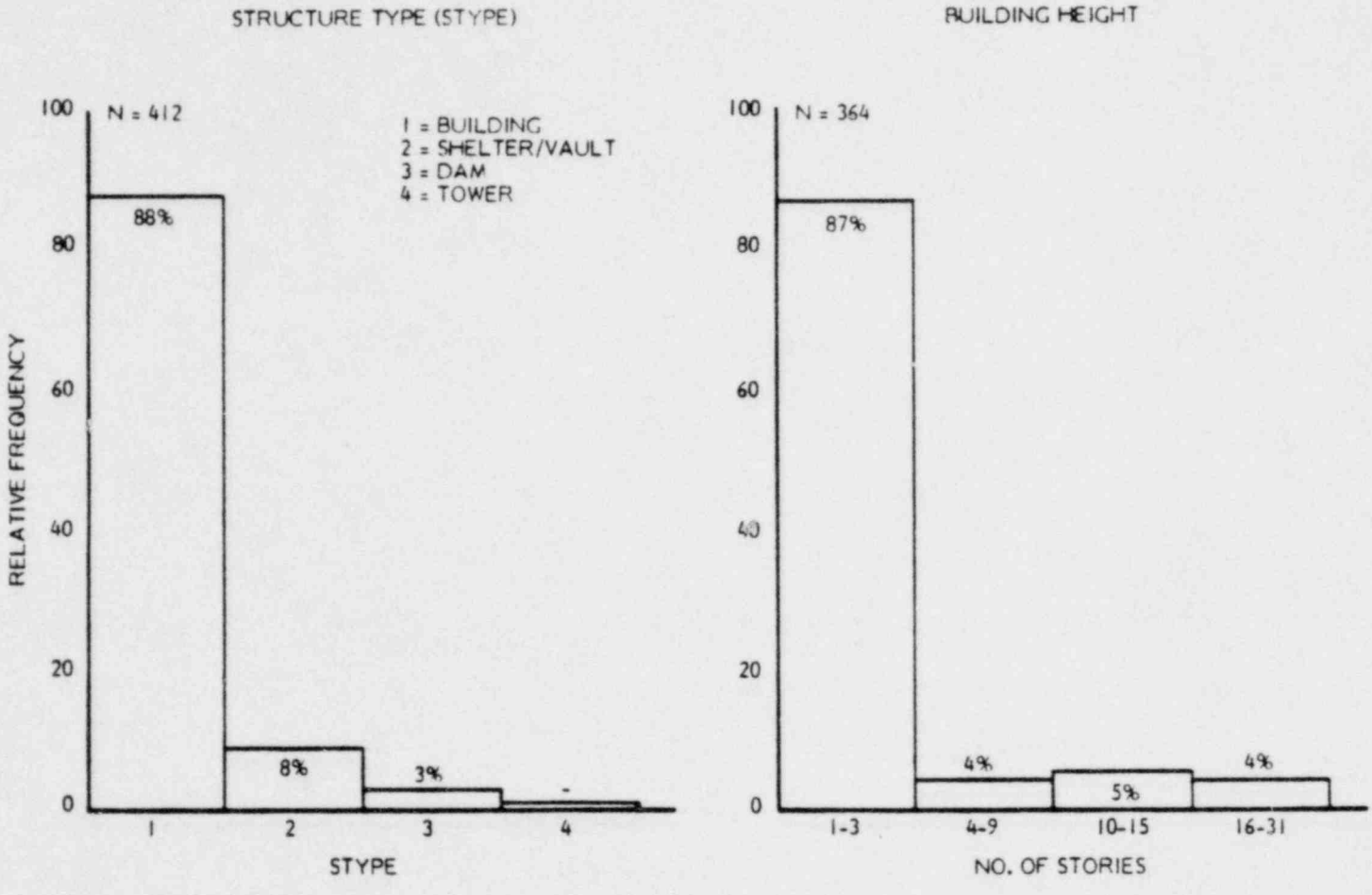

FIGURE A-4

DISTRIBUTION OF STRUCTURE TYPE AND BUILDING HEIGHT
FOR THE NEAR SOURCE STRONG MOTION DATA BASE

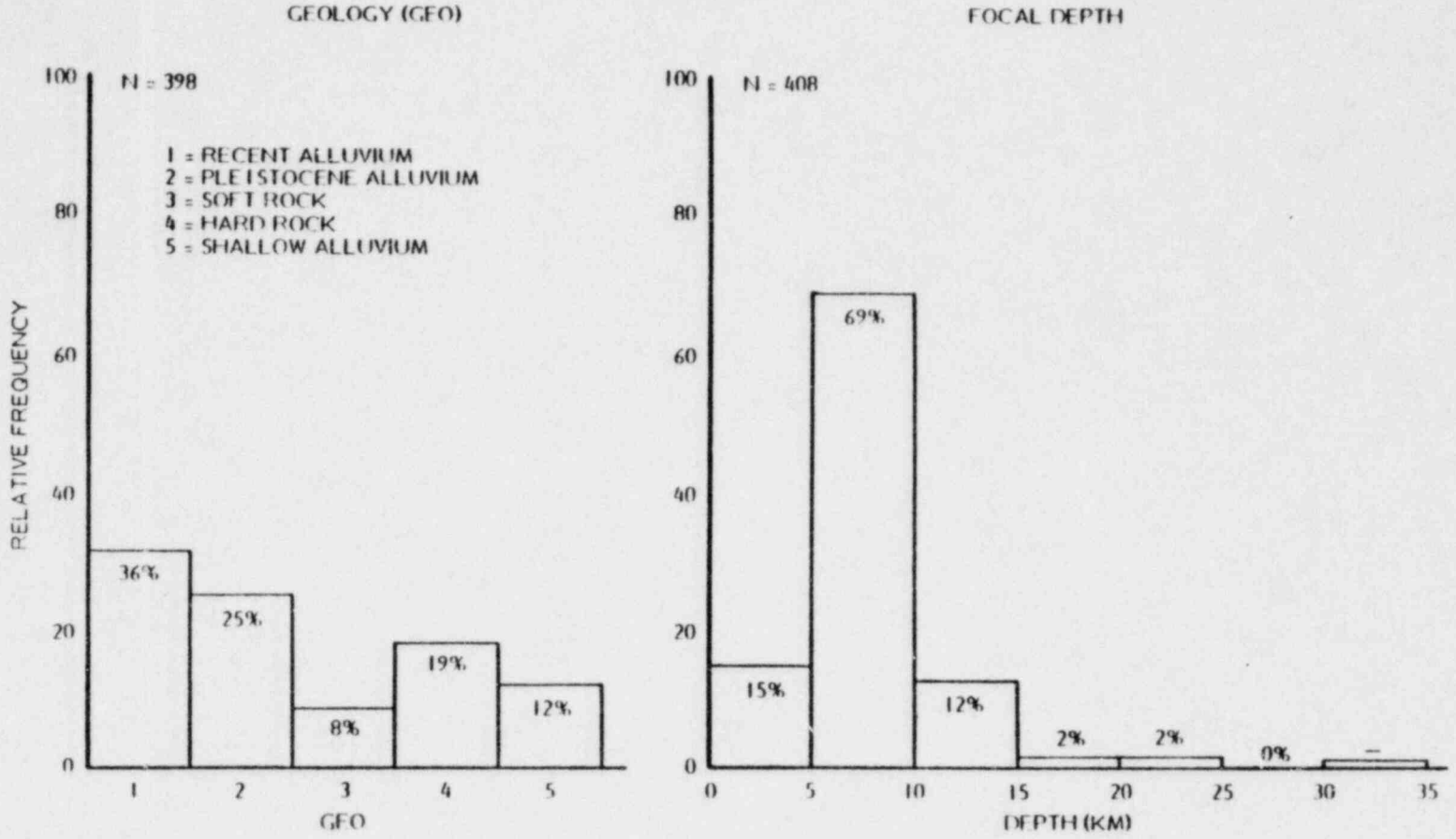

FIGURE A-5

DISTRIBUTION OF RECORDING SITE GEOLOGY AND EARTHQUAKE FOCAL DEPTH FOR THE NEAR SOURCE STRONG MOTION DATA BASE

Magnitude

The local Richter magnitude scale (M_L) was used as a uniform basis for characterizing earthquake size. Only those magnitudes equal to or greater than 3.5 were selected for analysis. (The strong motion data associated with smaller events are frequently plagued by large uncertainties and incompleteness.)

Source-to-Site Distance

Peak acceleration data recorded at distances of 0 to 20 km were selected for analysis. For earthquakes of $M_L < 5$, the epicentral distance was used so as to eliminate the large uncertainties associated with focal depth determinations. For the larger events, where significant rupture occurs, the distance closest to the zone of energy release was used (Boore, et al., 1978).

Site Geology

Strong motion data recorded at sites underlain by recent alluvium, Pleistocene (older) alluvium, soft (sedimentary) rock, and hard (crystalline) rock were selected to study the effect that geology might have on observed peak accelerations. Stations situated on shallow alluvium, or those having known topographic effects, were not considered appropriate for site-specific analysis.

Instrument Location

Peak acceleration data recorded on instruments located in basements of buildings and at ground level were selected to study the effect of embedment on the observed motions. Ground-level instruments included those located on the ground level of buildings without basements, free-field stations housed within small shelters, and a few located near the abutments of dams.

Other Recording Site Factors

No selection regarding building height or instrument type was made. The limited distribution of these characteristics precludes a statistical analysis of their potential effects.

Focal Depth

Consistent with regional seismicity and the crustal thicknesses of California, only shallow-focus earthquakes (less than 25 km deep) were used in the analysis.

Application of the above criteria resulted in the selection of 223 records (439 components) from 86 earthquakes considered appropriate for establishing an acceleration attenuation relationship for the SNM.

A.3 ANALYSIS OF ATTENUATION

A linear least-squares analysis was used to establish a site-specific attenuation equation for peak acceleration. The most general form of the regression equation used in the analysis was the logarithmic (base e) relationship:

$$\begin{aligned} \text{Ln PHA} = {} & A + BM_L + CM_L^2 + D\,\text{Ln}(R+1) + (E + F \cdot M_L)\,\text{Ln}^2(R+1) \\ & + G \cdot \text{LOC} + (H + I \cdot \text{Ln}(R+1))\,\text{RVSS} + \epsilon \end{aligned} \qquad \text{(A-1)}$$

where,

PHA = peak horizontal acceleration (g)

M_L = local earthquake magnitude

R = source-to-site distance (km)

LOC = recording instrument location

LOC = 0 : basement level

LOC = 1 : ground level

RVSS = recording site geology

RVSS = 0 : soil

RVSS = 1 : rock

A, B, . . .J = regression coefficients

ϵ = random error term

A weighted least-squares analysis was used in order to reduce the effect of two significant biases in the near-source data base: the first bias resulted from an overwhelming number of small magnitude earthquakes in the sample (Table A-1); the second bias was due to multiple recordings from the same earthquake (Table A-2). To account for these biases, it was decided that each magnitude range should carry an equal weight in the analysis and that, within a given range, each earthquake should be equally represented. This concept may be represented in the regression by use of a relative weighting factor of $1/n_i n_j$, where n_i is the total number of events in the i^{th} magnitude bin and n_j is the total number of peak acceleration components for the j^{th} earthquake within that bin. For an example of this procedure, refer to Tables A-1 and A-2.

The Oroville aftershock of September 26, 1975 is represented by 11 records, each having two horizontal components. Its magnitude (M_L 4.0) falls within the M_L 3.5-4.4 magnitude bin, which is represented by 50 earthquakes. Thus, for this event $n_i = 50$ and $n_j = 22$, corresponding to a relative weighting factor of 1/1100.

The weighted-regression analysis resulted in the following expression for peak horizontal acceleration:

$$\text{Ln PHA} = -5.06 + 0.69\, M_L - 0.40\, \text{Ln}\,(R + 1) + (0.016\, M_L - 0.13)\, \text{Ln}^2\,(R + 1) + 0.62\, \text{LOC} \qquad \text{(A-2)}$$

with a standard error of estimate of 0.61 and a correlation coefficient of 0.75.

TABLE A-1

NUMBER OF EARTHQUAKES
FOR GIVEN MAGNITUDE
INTERVALS

Magnitude Range M_L	Number of Events
3.5 - 4.4	50
4.5 - 5.4	25
5.5 - 6.4	11

TABLE A-2

SUMMARY OF EARTHQUAKES HAVING MULTIPLE RECORDINGS

Earthquake Name	Date (GMT) Yr-Mo-Day	Magnitude M_L	Number of Records
	M_L = 3.5 - 4.4		
Oroville	75-09-26	4.0	11
Oroville	75-08-11	3.6	10
Oroville	75-08-16	4.0	10
Oroville	75-08-03	4.1	8
Oroville	75-08-06	3.6	7
Bear Valley	73-06-22	3.9	6
Oroville	75-10-10	3.6	5
Oroville	75-10-28	3.5	5
Southern California	76-01-01	4.4	4
Oroville	75-09-12	3.5	4
Imperial Valley	77-10-28	3.9	3
Imperial Valley	77-11-14	3.9	3
Coalinga	75-01-06	4.4	2
Imperial Valley	77-10-30	4.0	2
Central California	67-12-31	4.3	2
Oroville	75-08-04	3.5	2
Imperial Valley	76-04-25	4.0	2
Cape Mendocino	75-01-12	4.4	2
Managua	72-01-03	4.1	2
Imperial Valley	75-06-20	4.2	2
	M_L = 4.5 - 5.4		
Oroville	75-09-27	4.6	10
Oroville	75-08-06	4.7	9
Oroville	75-08-03	4.6	8
Oroville	75-08-08	4.9	8
Hollister	74-11-28	5.2	4
Parkfield	75-09-13	4.8	3
Oroville	75-08-02	5.2	3
Brawley	75-01-23	4.8	3
Lytle Creek	70-09-12	5.4	3
Imperial Valley	74-12-06	4.5	3
Daley City	57-03-22	5.3	2
Oroville	75-08-02	5.1	2
Hollister	70-03-31	4.5	2
Northern California	77-06-21	4.6	2
Southern California	77-08-12	4.5	2
Central California	75-08-02	4.9	2

TABLE A-2

(CONT.)

Earthquake Name	Date (GMT) Yr-Mo-Day	Magnitude M_L	Number of Records
	M_L = 5.5 - 6.4		
San Fernando	71-02-09	6.4	10
Santa Barbara	78-08-13	5.7	5
Parkfield	66-06-28	5.5	4

Both the M_L^2 term and the effect of geology were found to be statistically insignificant at the 95 percent confidence level. The negligible effect of geology on the PHA was a surprising result. Many investigators in the past have found that, at distances less than about 30-50 km, rock tends to have higher accelerations than do soils, although these results have been statistically questionable. To check our results, the analysis was repeated, separating soils into recent and older alluvium, and rock into soft and hard rock. Again, no statistically significant effect was found, which might be explained by the type of geologic classification used. For instance, Seed, et al. (1975), who suggests that the depth of soil is important, found that peak accelerations recorded on stiff soils (less than about 50 m deep) are similar to those recorded on rock.

The most probable explanation for the relative insignificance of geology lies in the very strong effect of instrument location (i.e., the LOC parameter). This parameter, overlooked by past investigations, was found to be as statistically significant as the effects of magnitude and distance. Further, an interesting link was found to exist between LOC and geology. When LOC was left out of the regression analysis, a significant difference between rock and soil was found. After careful investigation, we found that rock sites were primarily located at ground level, representing LOC = 1. Therefore, the higher accelerations recorded on rock could be completely explained by the instrument location without including an effect for geology.

This conclusion was quite significant, and since the SNM is embedded, a careful analysis of the LOC parameter was carried out. Regression analyses done independently on recent and older alluvial soils gave almost identical results for the coefficient of LOC. Even when data were restricted to buildings of 1 to 3 stories in height, similar results were found. Therefore, we concluded that the importance of the effect of instrument location over geology was both credible and significant.